National Technical University of Athens
Department of Physics

CERN
BE-ABP-HSS

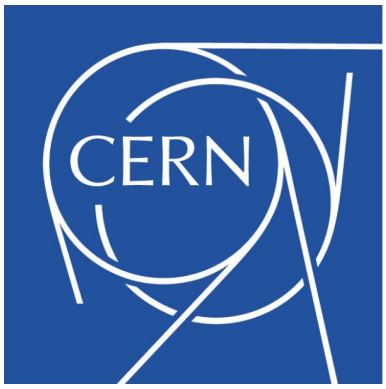

Master's Thesis in Advanced Physics

Beam dynamics studies at CERN proton synchrotron

Author: Myrsini Kaitatzi
E-mail: mirsini.kaitatzi@cern.ch

Supervisor: Dr. Alexander Huschauer
E-mail: alexander.huschauer@cern.ch

Academic Supervisor: Prof. Evangelos Gazis
E-mail: egazis@physics.ntua.gr

CERN Meyrin, may 1, 2019


CERN

Abstract

High-energy physics research has always been the driving force behind the development of particle accelerators. For this reason it was necessary to go to even higher energies. he main parameter which needs to get maximized is the luminosity. Luminosity depends on the number of particles per bunch (n1,n2), the bunch transverse size at the interaction point and the bunch collision rate (f). Luminosity L is given:

$$L = f\frac{n1n2}{4\pi\sigma_x\sigma_y}$$

The need of higher energy and higher intensity beams leads scientists to conceive new upgrade projects. The accelerators of the injector complex gave a decisive contribution to the excellent performance of the Large Hadron Collider (LHC) during its first run, which finished in February 2013, and was crowned with the discovery of the Higgs boson. The injectors had provided many different types of beams over a wide range of intensities, emittances and distances between bunches, which were crucial for safely commissioning. To reach the high luminosity, the CERN injector complex has to generate higher brightness and intensity beams. To this end, the Proton Synchrotron Booster (PSB), the PS and the Super Proton Synchrotron (SPS) are upgraded and consolidated and LINAC4 is constructed, during Long Shutdown 2 (LS2).

The Large Hadron Collider (LHC) is one of the largest scientific instruments ever built. To sustain its performance, the LHC will need a major upgrade in the 2020s. This will increase its instantaneous luminosity (rate of collisions). The goal of LHC Injectors Upgrade (LIU) project is to make the injectors capable of delivering reliably the beams required by the HL-LHC. For the production of the future HL-LHC (High Luminosity LHC) type beams, major upgrades are needed to eliminate the existing limitations, in particular related for example to space-charge.

Proton Synchrotron (PS) plays an important role in the production of the beams for the Large Hadron Collider (LHC), as its goal is to preserve at maximum the transverse emittances defined by its injector, the PS Booster (PSB). The current 1.4 GeV CERN PS injection energy limits the maximum intensity required by the future High-Luminosity LHC. The bare machine large chromaticity combined with the non-linear space charge forces make high-brightness and high-intensity beams cross betatron resonances along the injection flat bottom, inducing in this way transverse emittance blow-up and beam losses.

This Master thesis work has been carried out at CERN in the framework of the LHC (Large Hadron Collider) Injector upgrade (LIU) program. Experiments were carried out in order to identify the existing betatronic resonances of Proton Synchrotron (PS) by applying a large emittance, not space-charge dominated beam on a magnetic flat bottom at constant energy, leading to the observation of the tune diagrams. The results of measurements will be presented in this thesis.

Nomenclature

Acronyms

CERN	-European Organization for Nuclear Research
PS	-CERN Proton Synchrotron
PSB	-CERN Proton Synchrotron Booster
SPS	-CERN Super Proton Synchrotron
LHC	-CERN Large Hadron Collider
LINAC4	-Linear Accelerator 4
Linac	-Linear Accelerator
LIU	-LHC Injectors Upgrade
LS2	-Long Shutdown 2
RF	-Radio Frequency
SC	-Space Charge
WP	-Working Point
MAD	-Methodical Accelerator Design
FFT	-Fast Fourier Transform
FWHM	-Full width at half maximum
MTE	-Multi-Turn Extraction
LEQ	-Low Energy Quadrupoles
PFW	-Pole Face Windings

Constants

c	-Speed of light, $[3 \times 10^8 m/s]$
m_0	-Proton mass, $[1.673 \times 10^{-27}\text{kg}]$
e	-Elementary charge, $[1.602 \times 10^{-19}\text{C}]$
r_0	-Classical radius, $[1.54 \times 10^{-18}\text{m}$ (protons)$]$
ε_0	-Vacuum permittivity, $[8.854 \times 10^{-12}$ F/m$]$

Acknowledgments

Throughout the writing of this dissertation I have received a great deal of support and assistance.

Firstly, I would like to express my gratitude to my research supervisor, Dr. Alexander Huschauer , for giving me the opportunity to do research and providing invaluable guidance throughout this research at CERN. He has taught me the methodology to carry out the research and to present the research results as clearly as possible. I am extending my thanks to my section leader Massimo Giovannozzi for his support during my research work. Both of them have much inspired me due to their dynamism, vision, sincerity and motivation.

I wish to show my gratitude to my academic supervisor Evangelos Gazis for introducing me to my field area and support me throughout my studies. I would also like to thank my tutors, Dr. Alexandros A. Serafetinides and Dr. Mersini Makropoulou, for their helpful discussions, valuable counsels. They taught me and shared their invaluable knowledge throughout my studies. I got immense help in data collection from my professors who they succesfully provided me with the tools that I needed to choose the right direction and successfully complete my dissertation and studies.

I would like also to thanks the OP team for the support during the MDs and the SWAN team for the development of online Python notebooks used for data analysis.

At this point, I take the opportunity to sincerely acknowledge the European Organization for Nuclear Research (CERN), for performing all my research studies.

Nobody has been more important to me in the pursuit of this project than the members of my family. I am extremely grateful to my parents for their love, guidance, caring and sacrifices for educating and preparing me for my future. Most importantly, I am very much thankful to my brother whose advices and encouragement helped me excel in, hence advance my critical thinking.

I would like to say thanks to my research colleagues and friends from my internship at CERN, Efstathios Logothetis, Rafaella Eleni Kotitsa, Eirini Koukovini Platia, Fotini Asvesta, Haroon Rafique for their wonderful collaboration, constant encouragement, guidance and friendship . I would like to recognize the invaluable assistance that all of them provided during my work.

In addition, I extend my thanks to my friends Stella Tzioga, Georgia Kapnoulla for their support and encouragement during my internship.

Finally, it is a pleasant task to express my thanks to all those who contributed in many ways to the success of this study and made it an unforgettable experience for me.

Author

KAITATZI Myrsini

Contents

1 Introduction

1.1 CERN

CERN (the acronym for the French: Conseil Européen pour la Recherche Nucléaire) is the European Organization for Nuclear Research, situated on the Swiss-French border near Geneva.The CERN convention was signed in 1953 by the twelve founding states Belgium, Denmark, France, the Federal Republic of Germany, Greece, Italy, the Netherlands, Norway, Sweden, Switzerland, the United Kingdom and Yugoslavia, and entered into force on September 29, 1954. Today there are 23 member states.

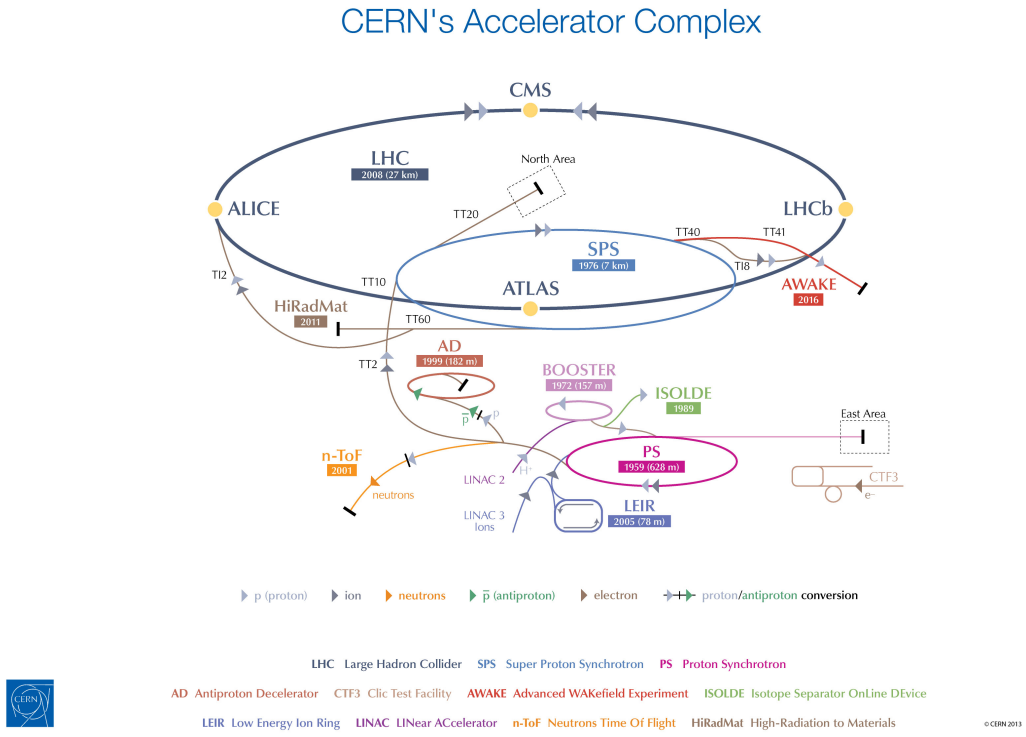

Figure 1: CERN accelerator complex.

The accelerator complex at CERN, detectors and other infrastructure are used by physicists to accelerate particles to high energies and through their collisions gain knowledge about the structure of matter. The complex is a succession of machines that accelerate particles to increasingly higher energies. In the Large Hadron Collider (LHC)– the last element in this chain – particle beams are accelerated up to the record energy of 6.5 TeV per beam. Most of the other accelerators in the chain have their own experimental halls where beams could also be exploited for experiments at lower energies. This thesis focuses on studying loss maps at low energy in the CERN Proton Synchrotron (PS) and give an overview of the various resonant conditions.

1.2 Introduction to accelerator physics

The most obvious components of particle accelerators and beam transport systems are those that provide the beam guidance and the focusing system of the beam. In a circular accelerator the beam of charged particles should follow the closed orbit. The basic structure of a synchrotron is composed by dipoles which curve the particles trajectory and by quadrupoles which focus the beam.

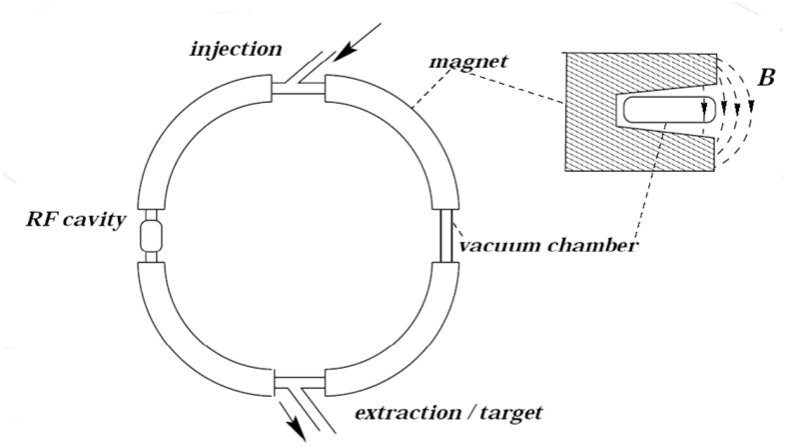

Figure 2: Main structure of a synchrotron.

The two main tasks of a circular accelerator are first to increase the particle energy and secondly to change the particle direction (follow a given trajectory, focusing). An accelerator is composed by structures to accelerate, steer and measure the particles. The force required to bend and steer the charged particle beam or provide focusing to hold particles close to the ideal path is known as the Lorentz force and are derived from electric and magnetic fields through the Lorentz equation. For a particle carrying a single basic unit of electrical charge the Lorentz force equation is expressed by:

$$F = eE + e[v \times B] = eE + evr \times B = F_E + F_B \tag{1}$$

, where e is the basic unit of electrical charge. The vector E is the electric field coming from the (RF) cavities, the vector B represents the magnetic field, and v is the velocity vector of the particle. The Lorentz force is applied as bending force in the magnets to guide the particle on a design orbit which ideally all the particle should follow. This force will also be used for beam focusing to confine a beam of particles to within a narrow vicinity of the ideal path. The evolution of particle trajectories under the influence of the Lorentz force is called beam dynamics.

Lorentz force indicates that electric force F_E can be applied to accelerate the particles into the direction of motion. In contrast, magnetic force F_B act orthogonal to the direction of motion and can thus be effectively exploited to deflect particles. Particles' velocity is close to the speed of light [c], so it is more feasible to use the magnetic field of 1[T], which gives the same bending power as en electric field of 3*108[V/m].

For this study, the magnetic elements are considered as purely transverse, two-dimensional fields in the coordinate system. Therefore we neglect the electric field and by considering a constant transverse magnetic field we divide by the velocity and get a relation between the magnetic field and the momentum p of the particle from which we obtain the expression of beam rigidity: $B\rho = p/e$, where p is the momentum vector and connects the magnetic dipole field needed for a circular orbit of radius ρ to the particles momentum and charge. As general rule in the arc section of a synchrotron the bending strength of a dipole is given by:

$$F_B = m\frac{v^2}{\rho} \rightarrow \frac{1}{\rho} = \frac{qB}{p} \leftrightarrow \frac{1}{\rho}[m^{-1}] \approx 0.3\frac{B[T]}{p[GeV/c]} \tag{2}$$

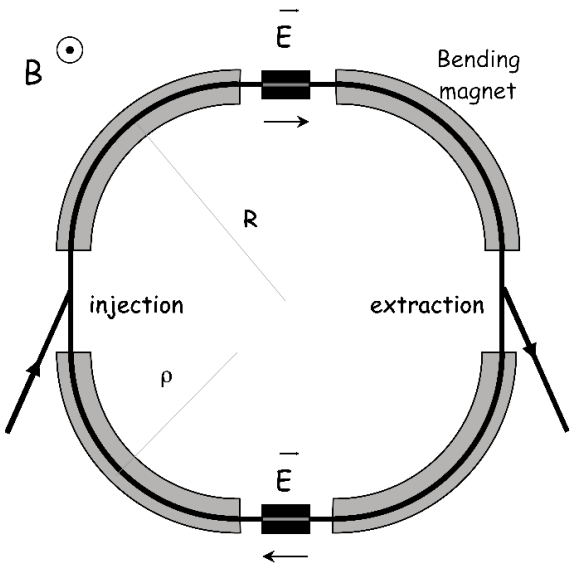

Figure 3: Synchrotron accelerating sections.

Synchrotron acceleration is performed by radio frequency (RF) cavities. The circular motion is ensured by a guide field F_B which provided by bending magnets with a homogenous field. Synchrotrons include some straight sections. In reality, the orbit in a synchrotron is not a circle, as is clearly depicted in Figure 3, straight sections are added for RF cavities, injection and extraction, etc. In the straight sections the accelerating elements and beam diagnostics devices are usually placed, as well as injection and extraction systems. At this point it should be mentioned that an important procedure is that the beam is pre-accelerated in a linac (or a smaller synchrotron) before injection.

Considering now a ring for particles with energy E with N dipoles of length L (or effective length l, i.e. measured on beam path) we retrieve equations concerning the bending angle $\theta = 2\pi/N$, and the bending radius $\rho = l/\theta$. The bending radius ρ does not coincide to the machine radius $R = L/2\pi$. The integrated dipole strength then is given by the equation: $Bl = 2\pi p/Nq$. It may simply deduced from the previous equations that by choosing a dipole field, the dipole length is imposed and vice versa. They also reveal that the higher the field is, the smaller number of dipoles can be used.

2 Relevant Concepts of beam dynamics

In a synchrotron charged particles are traveling on a fixed orbit. Magnetic fields are used to keep them on the wanted trajectory, while (RF) cavities provide the accelerating logitudinal electric field. As the particles gain energy, the magnetic fields are adjusted synchronously so that the orbit remains unchanged. In order to guide and focus the particles during their accelaration in a synchrotron we construct repetitive pattern of magnetic elements separated by straight sections, which constitute the lattice of the accelerator. The lattice cell is the special magnet arrangement of the principle building block in an accelerator.

At any instant, particles may be displaced horizontally by x and vertically by y from the ideal position and may also have divergence angles horizontally and vertically with respect to the designed orbit. Generally, the particle motion is separated into longitudinal motion: motion tangential to the reference trajectory along the accelerator structure, u_s and transverse motion: degrees of freedom orthogonal to the reference trajectory, u_x, u_y. This chapter introduces the basic concepts of both longitudinal and transverse beam dynamics of charged particles in the machine.

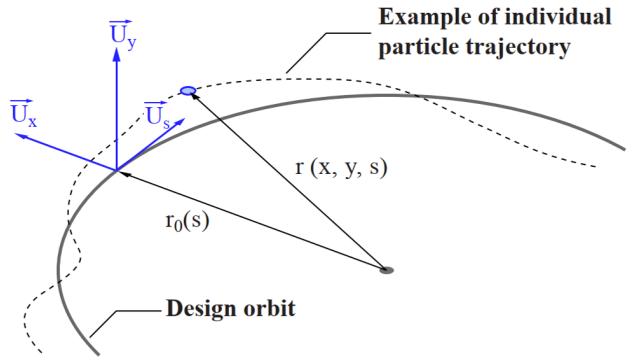

Figure 4: Coordinate system. us, ux, uy are unit vectors in a moving coordinate system, following the particle. Designed orbit is defined by the dipole magnets and is the trajectory which the ideal particle should follow.

2.1 Transverse betatron motion

A synchrotron consists of dipoles to provide a closed path (nominally circular), quadrupoles to provide transverse focusing, and drift spaces. Dipoles and quadrupoles form the linear elements of the lattice.

Dipolar vertical magnetic fields $B_y = k_1 p/q$ curve the reference orbit leading to the local bending radius $r_0(s)$. Quadrupole magnets, are periodically arranged with alternating strenght polarities. To avoid a blow-up of the beam, quadrupolar magnetic fields $B_x = yk_2 p/q$, $B_y = -yk_2 p/q$, are used. They steer particles towards the reference orbit in the focusing plane and simultaneously away from the orbit in the other plane, the defocusing one. Conventionally, a quadrupole magnet with positive strength $k_2 > 0$ focuses in the horizontal plane and is hence referred to as a focusing quadrupole. Focusing fields also provide the closed orbit of the particle, this is the trajectory that closes upon itself, and it is what we observe out of the Beam Position Monitors (BPM) readings of the stored beam. Generally, closed orbit is defined as the path of a single particle averaged over many turns in the machine.

Under the influence of the focusing fields the particles follow a certain path along the machine. Each particle executes transverse betatron oscillations, with its own amplitude and phase, which are different from each particle. As the particles move around the accelerator , whenever their divergence (angle) causes them to stray too far from the central trajectory the quadrupoles focus then back towards the central trajectory. In 19th century George William Hill, one of the greatest master of celestial mechanics of his time, studied the differential equation for motions with periodic focusing properties. Transverse motion calculations in linear beam optics are formed by the following two Hill's equations:

$$x''(s) + \left(\frac{1}{R^2(s)} - k(s)\right) x(s) = 0 \tag{3}$$

$$y''(s) + k(s)y(s) = 0 \tag{4}$$

with $R(s)$ being the bending radius having consequently $1/R(s)$ being zero in the vertical plane and $k(s)$ is the quadrupole strength which is equal to $k(s) = \frac{G}{B\rho}$, and the quadrupole gradient G is defined as $G = \frac{\partial B_x}{\partial x}$. These two equations describe the transverse motion for a particle traveling through the magnetic structure of an accelerator. These two coordinates represent the transverse plane of the beam. The extra terms in the horizontal plane comes from the bending magnets that do not take place in the vertical plane. The term $1/R^2(s)$ corresponds to the dipole weak focusing. It is impressive that even without quadrupoles there is retrieving force (focusing) in the bending plane of the dipole magnets.

2.1.1 Betatron tunes

The general solution of Hill's equation:

$$x(s) = \sqrt{\epsilon}\sqrt{\beta(s)}\cos(\mu(s) + \mu_0) \tag{5}$$

$$\mu(s) = \int_0^s \frac{ds}{\beta(s)} \tag{6}$$

Where $\mu(s)$ is the phase advance of the oscillation between the points 0 and s along the lattice. A single particle will perform transverse oscillations and so the single particle trajectories will oscillate around their closed orbit. These transverse oscillations are called Betatron Oscillations, and they exist in both horizontal and vertical planes. The number of such oscillations/turn is called tune and for one complete revolution, corresponds to the $\mu(s)$ when normalised to 2π.

$$Q = \frac{1}{2\pi}\int \frac{ds}{\beta(s)} \tag{7}$$

There is a tune for the horizontal (Q_x), the vertical (Q_y) and the longitudinal (Q_s) oscillation. In general, the position of the particle in the transverse motion characterized by two things: displacement from central path, and angle with respect to central path.

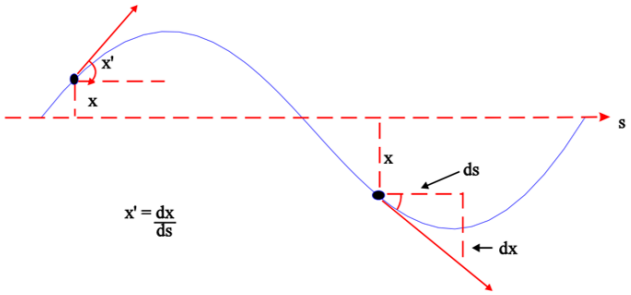

Figure 5: Transverse position and angle displacement for a particle moving around the accelerator.

The phase space coordinates (x, x') of a single particle at a given location s of the machine lie on the phase space ellipse when plotted for several turns. The lattice thus the arrangement of the magnets is responsible for the orientation and the shape of the ellipse. The area of the ellipse is furthermore equal to $\pi\epsilon$, which, according to Liouville's theorem, is a constant of motion as long as only conservative forces are present and the energy of the particle remain constant. Hence, as we move around the ring, $\beta(s)$ varies and alters the shape of the ellipse, but the area of the ellipse remains constant all around the accelerator. The term is referred to as emittance with mm*mrad being its unit and is determined solely by initial conditions. The beam emittance describes the quality of the particle ensemble. he area in phase space and can be considered like the temperature of a gas. The lower the emittacne the better the beam quality. Together with the beta function it defines the beam dimension.

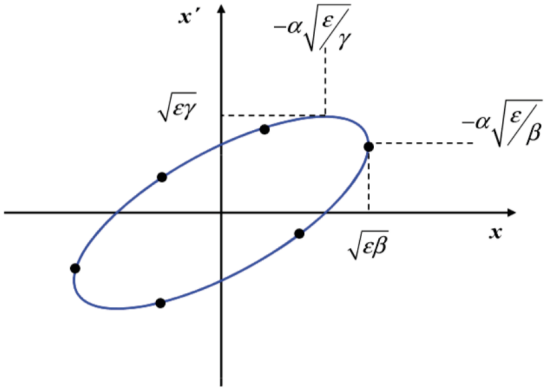

Figure 6: Transverse phase space plot. The transverse motion is being represented on a "Phase plot", points on the ellipse represent different turns of the particle.

In an ideal storage ring, if there is no beam energy change, the area of the ellipse in the phase space is constant. Neglecting also higher order magnetic fields and other coupling mechanisms, the horizontal, vertical and longitudinal phase space can be treated independently and, therefore, one can define an emittance in each plane.

2.1.2 Linear imperfections

Imperfections (= errors) in the real accelerator optics can be introduced by uncertainties or errors on: beam momentum, magnet calibrations and power converter regulation. Alignment errors are also a common source of imperfections.

The first category of imperfections that beam encounters when is first injected is the presence of an unintended deflection along the paths. How can an unintended deflection appear? The first source is a field error (deflection error) of a dipole magnet, which can occur be due to an error in the magnet current. The second source is a misalignment of a quadrupole magnet. To this end, dipole orbit correctors are installed to compensate the effect of deflections. Orbit correctors, generate a deflection of opposite sign and amplitude that compensates locally this imperfection.

At this point it would be important to mention that particles inside the beam have not the same momenta, thus there is a relative momentum deviation in the beam. Particles with different momenta follow different trajectories in a dipole field whose amplitude is called dispersion. Let's consider two particles with different momentum p0,p0+p, a dipole with field B and a bending radius ρ. Magnetic rigidity is given by $B\rho = \frac{p_0}{q}$, and for off-momentum particles $B(\rho + \Delta\rho) = \frac{\rho_0 + \Delta p}{q} \rightarrow \frac{\Delta\rho}{\rho} = \frac{\Delta p}{p_0}$. Consider now the effective length of the dipole unchanged $\theta\rho = l = const. \rightarrow \rho\Delta\theta + \theta\Delta\rho = 0 \rightarrow \frac{\Delta\theta}{\theta} = -\frac{\Delta\rho}{\rho} = -\frac{\Delta p}{p_0}$. We end up getting the different deflection (different orbit) of the off-momentum particles $\Delta\theta = -\theta\frac{\Delta p}{p_0}$.

The resulting inhomogneous Hills equation, is extended to:

$$x''(s) + \left(\frac{1}{R^2(s)} - k(s)\right)x(s) = \frac{1}{R(s)}\frac{\Delta p}{p} \tag{8}$$

$$y''(s) + k(s)y(s) = 0 \tag{9}$$

Where the term $\frac{1}{R^2(s)}$ corresponds to the dipole week focusing and $\frac{1}{R(s)}\frac{\Delta p}{p}$ represents off-momentum particles. The solution of (8) can be written as

$$y(s) = y_b(s) + y_D(s) = \sqrt{\epsilon}\sqrt{\beta(s)}\cos(\mu(s) + \mu_0) + D(s)\frac{\Delta p}{p} \tag{10}$$

We can introduce the dispersion function D(s) that describes the local dispersion which, multiplied by the relative momentum deviation, creates an equilibrium orbit displaced from the central orbit. In particular $y_D(s)$ is the solution of the inhomogenous differential equation (10), the dispersion function must satisfy

$$D'' + K(s)D = \frac{1}{\rho(s)} \tag{11}$$

Dispersion is created by the momentum dependency of the bending radius in dipole magnets and appears therefore only in the plane of bending (generally the horizontal plane).

Another imperfection one should notice concerns errors excisting in quadrupole strengths (random and systematic). This has as an impact the change of the oscillation period, thus the modification of the tune Q. In a ring a focussing error affects the beam optics and envelope (size of the beam) over the entire ring.

In an accelerator in order to avoid further beam losses (because of cromatic errors, that will be explained in the next chapter) dedicated skew quadrupoles are installed in order to compensate for alignment errors. This is just a quadrupole which has been rotated by 45° about it's longitudinal axis. Betatron motion is coupled in the presence of skew quadrupoles. This rotation has the effect that a horizontal displacement induces a horizontal deflection. Therefore this skewed quadrupole no longer focuses (or defocuses) the beam, but transfers energy from one transverse plane to the other. Any quadrupole, which is not perfectly aligned, will have a skew component and will excite coupling. Generally the rotation of a quadrupole, even if it is minor, leads to coupling of the x and y planes and finally the field contains a skew component.

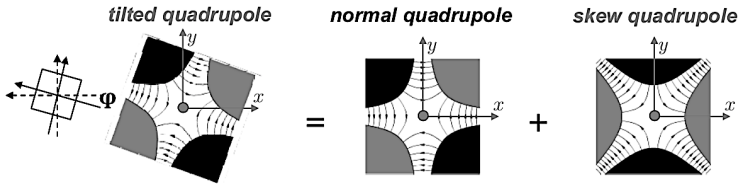

Figure 7: Skew components in the field generated out of skew quadrupoles.

Coupling errors lead to transfer of horizontal betatron motion and dispersion into the vertical plane. In other words, it leads to an exchange of energy between the two transverse planes and apparently to particle losses. Tune-shift, beta-beating, excitation of integer and half integer resonances are the outcome of these imperfections.

2.1.3 The working diagram and resonances

Perturbation terms in the equation of motion can lead to beam's instability are called *resonances*. Using the Hamiltonian formalism, the general resonance condition can be written as $n_x Q_x + n_y Q_y = l$, where n_x, n_y and l any three integers, and $N = |n_x| + |n_y|$, is the order of the resonance and can directly defines the principal driving multipole, which has 2N poles(N = 1 dipolar, N= 2 quadrupolar, N= 3 sextupolar, ...), which represent the field generating it. The resonance lines are represented in the tune diagram, imposing restrictions on the working point choice. Resonances where both n_x and n_y are positive are referred to as coupling resonances. The resonance excitation is then sensitive to systematic errors in the accelerator lattice. These resonances are called systematic or structured resonances and are likely to be strong. For a resonance of order N, if n_y is even then it is associated to a normal resonance. While if n_y is odd, the resonance is a skew resonance (driven by a skew N-multipole). The lowest order coupling resonance is referred to as linear coupling resonance, with the resonance condition $Q_x \pm Q_y = l$.

The tune is defined by the quadrupole arrangement and strength around the machine. The position of the tunes in a diagram of horizontal versus vertical tune is called a working point (Q_x, Q_y).

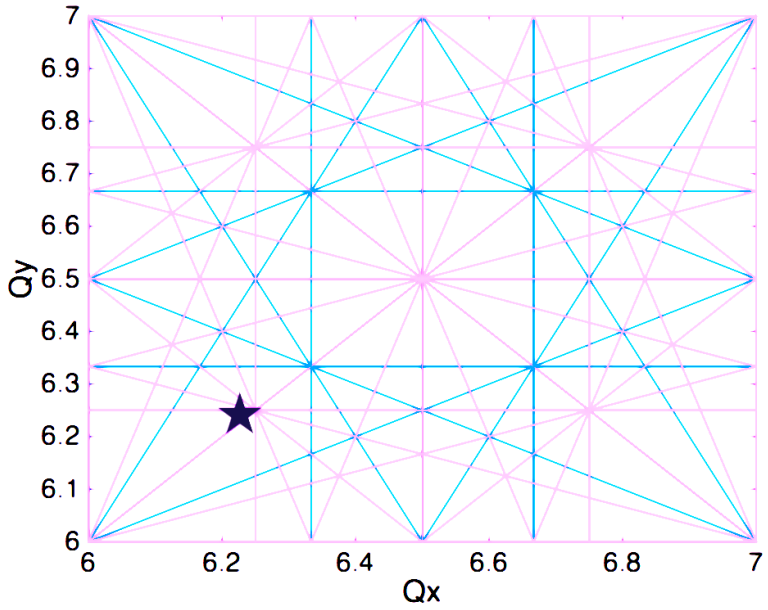

Figure 8: Tune diagram, the horizontal axis represents the horizontal tune, the vertical axis represents the vertical tune. Resonant lines up to 4th order. Random resonances represented in purple colour, while systematic ones in blue. The illustrated star, represent potential operational Working Point(WP).

For transverse betatron oscillations a betatron condition is that: After a certain number of turns around the machine the phase advance per turn of the betatron oscillation is such that the oscillation exactly repeats itself.

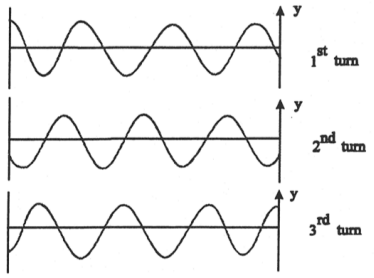

Figure 9: After 3 turns the betartron oscillation will exactly repeats itself.

The appearance of resonances is generally restricted only to circular accelerators due to the fact that the perturbations occur periodically at every turn. The resonance driving terms can appear from lattice periodicity and machine imperfections, such as magnetic field errors , power supply ripples. Another important factor leading to reasonances is the magnet misalignments. This phenomenon could also lead to feed-down effects. During normal operation resonance compensation is mandatory to avoid an emittance increase (leading the beam to blow-up). These lines cannot realistically be avoided, but, depending on their strengths and order, the influence on the beam can be minimized using dedicated multipole correctors.

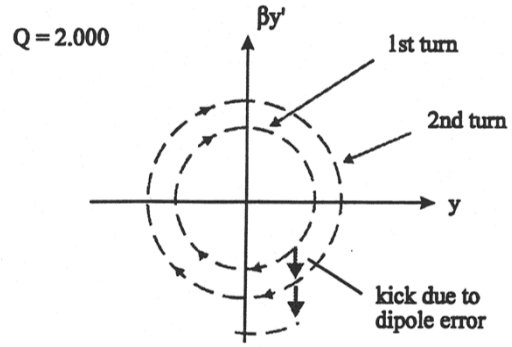

Figure 10: For $Q = 2.00$ the oscillation amplitude grows on each turn and the particle eventually be lost.

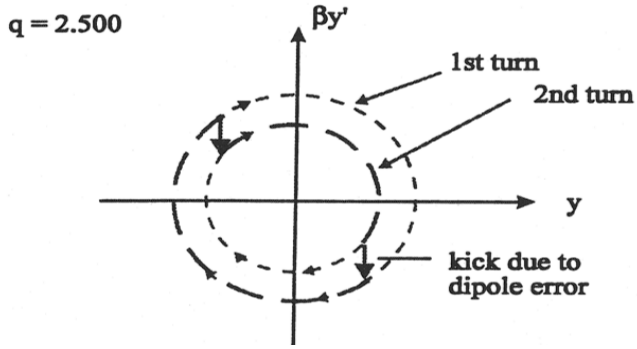

Figure 11: For $Q = 2.50$ the oscillation is cancelled out every second turn and the particle motion is more stable.

To avoid resonance conditions the frequency of the transverse motion must not be equal to (or a integer multiple of) the revolution frequency. When the tune is an integer number, the deflections add up on every turn. That leads amplitudes to diverge, the particles do not stay within the accelerator vacuum chamber. This is the first resonance that could be encountered, the integer resonance that occurs when $Q = l$. For half integer tune values $Q = l + 0.5$, the deflections compensate on every other turn. The amplitudes are stable, which looks like a much better working point for Q. We set now the machine tune to a quarter integer value: $Q = l + 0.25$ For quarter tune values, the deflections compensate every four turns thus the amplitudes are stable, and yet another a reasonable working point for Q.

2.2 Non-linearities

The non-linear resonances are those of third-order and above, driven by non-linear multipoles. Non linear elements such as sextupole magnets can have significant impact on the particle motion.

At this point it would be interesting to describe the hamiltonian of the non linear betatron motion. In a lattice made from dipoles and quadrupoles the Hamiltonian reads (in our usual coordinate system):

$$H(s) = \frac{\overline{p_x}^2 + \overline{p_y}^2}{2} - \frac{x^2}{2\rho(s)^2} + \frac{k_1(s)}{2}(x^2 - y^2) \tag{12}$$

where $\overline{p_x} = p_x/p_0$ and $\overline{p_y} = p_y/p_0$. The first term of Hamiltonian constitutes the kinetic term and the rest terms compose the vector potential accounting for the magnetic fields. Especially, $\frac{x^2}{2\rho(s)^2}$ refers to a dipole term and $\frac{k_1(s)}{2}(x^2 - y^2)$ to a quadrupole one.

The Hamiltonian for the nonlinear betatron motion is written like this

$$H(s) = \frac{\overline{p_x}^2 + \overline{p_y}^2}{2} - \frac{x^2}{2\rho(s)^2} + \Re \sum_{n=1}^{M} \frac{k_n + ij_n}{(n+1)!}(x + iy)^{n+1} \tag{13}$$

after a multipole expansion. We define H_0:

$$H_0(\overline{p}, \overline{q}; s) = \frac{p_x^2 + p_y^2}{2} - \frac{x^2}{2\rho(s)^2} + \frac{k_1 x^2 - k_1 y^2}{2} \tag{14}$$

the linear part (dependent only on dipoles and normal quadrupoles) and V :

$$V(\overline{p}, \overline{q}; s) = \Re \sum_{n2} \frac{k_n + ij_n}{(n+1)!}(x + iy)^{n+1} \tag{15}$$

the nonlinear part dependent on the nonlinear multipoles. The k_n,j_n form the normal and the skew multipoles coefficients respectively, where $k_n = \frac{1}{B_0\rho_0}\frac{\partial^n B_y}{\partial x^n}$,$j_n = \frac{1}{B_0\rho_0}\frac{\partial^n B_x}{\partial y^n}$.

Looking now the tune diagram one could see the resonance lines which are driven by a particular pattern of multipole field error. These lines have a finite width depending on the strength of the error. Thus a tune spread is generated among the particles in the beam. Once beam has been accelerated the problem becomes one of reducing all effects which produce a spread in Q. But firstly, one must correct the tune spread due to momentum: the chromaticity. Chromaticity is a focusing problem. Particles in a bunch have different momenta leading to have different tunes from each other. The chromaticity is defined as the derivative of the tune with respect to the momentum deviation $Q'_z = \frac{\partial Q_z}{\partial \delta}$. Sextupoles are special magnets magnets having non-linear fields and are used to compensate chromaticity. Sextupoles are inserted in the accelerator's lattice to correct the natural chromaticity produced by the focusing elements. In a sextupole a charged particle passing off-center receives a kick proportional to the square of its displacement from the center. However, one should consider that non-linear fields can lead to particle losses and hence to beam loss.

At this point, it would interesting to note that there are couple of applications making use of resonances. Paradoxically, some sets of multipole magnets are often required in a synchrotron to deliberately excite non-linear betatron resonances. Resonances can be exploited to extract the beam in a controlled way. For example in order to extract the beam in a long slow spill CERN scientists use 3rd order resonances. Also they use the 4th order resonances for the multi-turn extraction (MTE) scheme, which was invented to transfer the beam over 5 turns from the PS to the SPS at CERN with minimal losses. Resonant Multi-Turn Extraction (MTE) proposed in 2001 to reduce losses (compared to what was observed in previous extraction schemes), at PS to SPS transfer. Last but not least, for efficiently extract particles, a resonant fast extraction technique is used based on excitation of the half integer resonance by octupoles and a fast discharge of a quadrupole that pushes the particle tune onto the resonance so that they are extracted on a few ms.

To summarise, the number of resonance lines in tune space is infinite: any point in tune space will be close to a resonance of some order. Accordingly, stability of particles is far from smooth to be preserved. Resonances can be excited by nonlinear elements installed intentionally (e.g. sextupoles for chromaticity correction) and/or by unavoidable multipolar errors from magnet imperfections. Apart from non-linear fields there are also various collective effects that may lead to instabilities of particle bunches.

2.3 Space charge

Interactions between particles and the beam surrounding should not be neglected. If one examine the bunch as a whole can observe the collective effects. The most fundamental collective effect in particle accelerators is the SC, which can alter the dynamic behaviour of the beam. Its impact is generally proportional to the beam intensity and the main idea is that the current of the beam create self-fields and image fields.

This influences the coherent oscillations of the beam as a whole. There are two categories space charge effects are divided into, direct and indirect. The direct space charge effects are due to the fields generated by the beam itself. While the indirect effect, also called image effect, are due to the image charges formed at the surface of the beam pipe. It is beyond the scope of this study to examine the SC effect but nevertheless its existence is considerable in our studies.

Tune spread is mainly caused because of the SC effect in the PS leading to crucial constraints of selecting the proper bare working point. Selecting a working point aims to have the beam operating in a vicinity free of resonances eliminating in this way the potential to cross a dangerous magnetic resonant line.

The tune spread due to space charge has the shape of a necktie. The space charge necktie is the static picture of the tune spread. Particles oscillate as well in the necktie due to the synchrotron motion. Particles which exist in the core of the beam have small amplitude oscillations. The large amplitude particles get detuned the least and are at the higher part of the necktie, while particles which exist at the lowest part of this necktie get detuned the most. The core of the beam (small amplitude particles) are at lowest part of this necktie as they get detuned the most.

To conclude, it would be worth mentioning that very bright beams have a large space-charge tunespread, leading them to overlap with a number of machine resonances and this in turn causes emittance growth and beam loss, making the space charge one of the main limitations of the LHC injectors complex.

2.4 Longitudinal beam dynamics

In order to accelerate the beam particles we need a longitudinal electric field. Magnetic field cause deflection to the particle trajectory but they do not change the particle momentum. From the expression of the Lorentz force 1, now we take into consideration the term of electric field. The acceleration in synchrotrons is achieved through Radio-Frequency (RF) cavities. A radio frequency (RF) cavity is a special type of resonator. In synchrotrons RF cavities provide also longitudinal focusing.

To perform acceleration, without changing the bending radius ρ, a longitudinal voltage should be generated, which is applied in the vacuum chamber. Particle's momentum will be incremented on each turn by a precise voltage: $V = V_0 \sin\phi_s = V_0 \sin(\omega_{RF} t)$. The amplitude V_0 is pre-programmed and ϕ_s is the synchronous phase . Now particles experience a longitudinal motion which is called synchrotron motion. To synchronize the particles' revolution frequency ω_{rev} with the RF frequency ω_{RF} the following condition must be fulfilled: $\omega_{RF} = h\omega_{rev}$ The integer h is referred to as the harmonic number which defines the number of stable RF areas around the ring. In other words, defines the maximum number of bunches circulating in one revolution period in the machine.

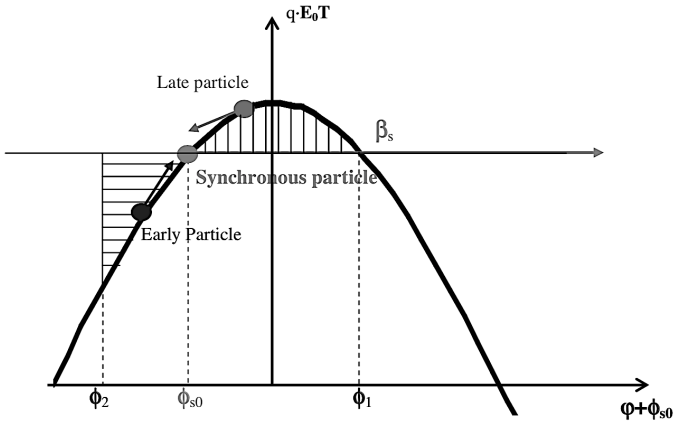

Figure 12: The synchronous phase of the synchronous particle is a stable point situated between $\pi/2$ and 0.

The synchronous particle is defined as the "virtual" particle which has the nominal momentum p0, trajectory and frequency and experiences always the same voltage phase $\phi(t) = \phi_s$ when it passes through the cavity. The other particles are asynchronous and will generally arrive sooner or later in the cavity, experiencing at each turn a different voltage and performing oscillations around ϕ_s. The change in revolution frequency Δf_{rev} of a single particle is related to its momentum offset through the slippage factor η : $\eta \frac{\frac{\Delta f_{rev}}{f_{rev}}}{\frac{\Delta p}{p_0}} = \frac{1}{\gamma^2} - \alpha_c \quad \text{with} \quad \alpha_c = \frac{1}{\gamma_t^2}$, where α_c is a machine property, the momentum compaction factor.

By the time $\eta = 0$ the beam reaches the transition energy $\gamma_{tr} = \frac{1}{\sqrt{a}}$. Above transition energy ($\eta < 0$), particles with lower momentum have higher revolution frequency than that of the synchronous particle. On the other hand, below transition energy ($\eta > 0$), particles with higher momentum have higher revolution frequency and arrive slightly sooner compared to the synchronous one. For this reason it experiences a negative kick thus feels an decrease in momentum. Consequently at the next turn this particle arrives a bit earlier than previously with respect to the synchronous particle. This time will feel a smaller negative kick by the RF voltage. When the phase offset with respect to the synchrotron phase $\Delta\phi = \phi - \phi_s$ changes sign, the particle gets a positive kick and is accelerated. This creates a stable oscillating motion around the synchronous particle, which is the "virtual" particle with constant revolution frequency ω_0 and energy offset $\Delta E = E - E0 = 0$.

At this point it would be worth-mentioning that PS was the first accelerator to have beams successfully crossing the transition energy, shortly after its commissioning in 1959. Therefore, the longitudinal dynamics are quite different below and above the transition energy.

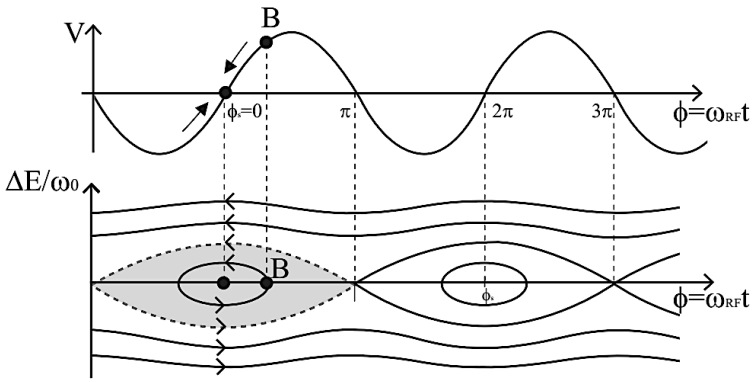

Figure 13: Top, the RF voltage waveform. Bottom: The iso-Hamiltonian trajectories in the $(\phi, \frac{\Delta E}{\omega_0})$ phase space that define the bucket, in shadowed area, and the separatrix, the dashed black contour. The particle B performs a synchrotron oscillation inside the bucket, in this case without acceleration ($\phi_s = 0$) and below transition energy ($\eta > 0$).

In Figure 13, the contour surrounding bucket is called separatrix and divides the stable from the unstable part of the motion. The area that the particles distribution occupies in the longitudinal phase space is called longitudinal emittance and is expressed in electron-Volt-second [eVs]. The area of the bucket is called acceptance.

As for the synchrotron tune Q_s, which describes the number of synchrotron oscillations per turn, can be defined as: $Q_s = \frac{\omega_s}{\omega} = \sqrt{h\frac{e\hat{V}|\eta\cos\phi_s|}{2\pi\beta^2 E}}$.

Finally, it could be easily assumed that longitudinal and transverse motions can be coupled. Nevertheless, for an easier understanding, and because the coupling is often very weak, the longitudinal and the transverse motions are usually treated as uncoupled, as we will do for these studies.

3 The CERN Proton Synchrotron

The CERN Proton-Synchrotron consists part of both the ion and the proton injection chain. Is a versatile machine that has accelerated different kind of particles up to different energies with a large range of beam intensity. PS has a circumference of 628m and operates at an energy of up to 26 GeV since 1959. This year 2019, PS celebrates the 60th anniversary since the accelaration of the first beam. It is the first accelerator to apply the alternating gradient principle by using one hundred combined function magnets. Each magnet is equipped with a main current circuit and five auxiliary current-circuits, which allows controlling the linear and non-linear magnetic fields. Main components of the PS will be presented in this chapter together with the dedicated instruments having being installed at the magnets and providing us information about the beams' characteristics. Last but not least it will be discussed the contribution of the PS to the LIU project.

3.1 Main components of PS complex

The main magnetic part of the Proton Synchrotron is a structure of 100 combined-function dipoles placed in a tunnel that forms a ring of 200 m in diameter. This structure comprises 100 combined-function magnet units (MU) each composed of of 10 blocks, of which 5 are "open" and 5 are "closed", as we see in Figure 14. Each magnet has a focusing (F) half-unit and a defocusing (D) half-unit . Which means that five provide a focusing strenght and five defocussing one. Main magnet units provide bending and focusing forces so as small-intensity beams can be accelerated to nearly top energy, even without additional auxiliary magnets. Between two subsequent magnet units, there is an interval called 'straight section', which is field-free so that the recurrent pattern is 'FOFDOD'. The straight sections are used for placing accelerating cavities, beam diagnostic devices, injection and extraction elements, and magnetic lenses.

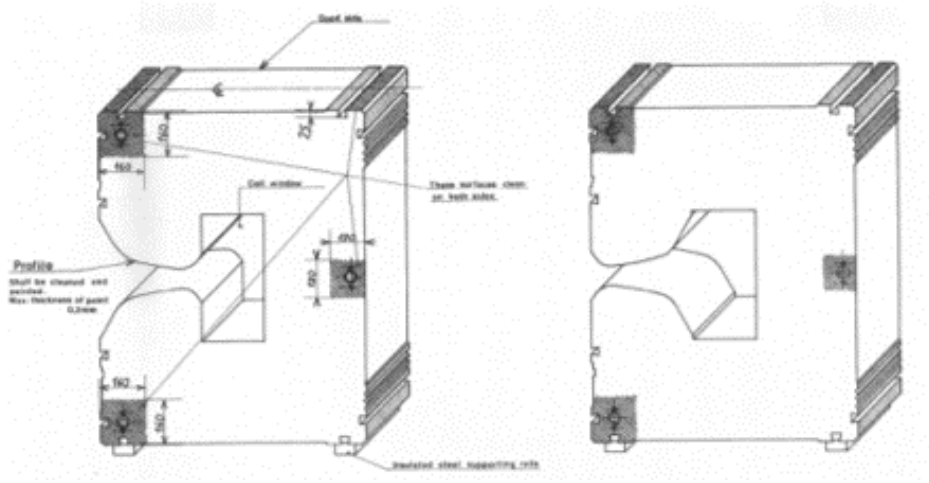

Figure 14: Open and closed single block of the main magnet units.

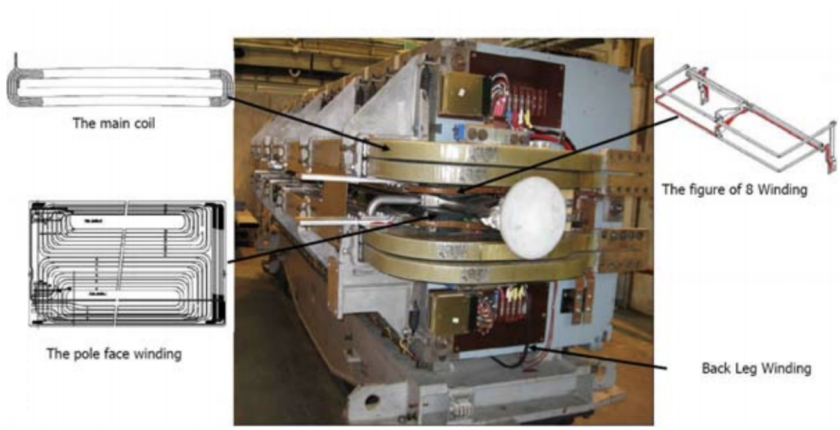

Figure 15: One out of 100 main magnets and drawings of the PFW, the F8L and the main coil [5].

Main magnets use does not provide sufficient control over important machine parameters such as the working point. Additional circuits have been mounted to the main magnets in order to give more degrees of freedom to the machine. Four of these auxiliary circuits are located on top of the magnet poles, and consequently called Pole Face Windings (PFW). PFW create an additional magnetic field in order to compesate distortions in the main field. They can also be used to correct undesired field components at low fields, e.g, due to eddy currents. There is also another auxiliary circuit in the shape of the number eight, called the Figure of Eight Loop (F8) which gives at the same time an additional degree of freedom.

The four original PFW circuits and the Figure-of-eight, five parameters became available to control and correct tune and chromaticity at high energy. On the other hand, at low energy between injection at 1.4 GeV (kinetic energy) up to about 4 GeV/c, the tune of the machine is controlled by two families of dedicated quadrupoles. These additional quadrupoles are distributed along the machine and allow us to move the working point to areas in the tune diagram which are more beneficial regarding betatronic resonances. In view of the 2 GeV injection energy upgrade, the control and correction of the working point and chromaticities would therefore become inevitable thus the selection of the tunes should be in that way so as to avoid resonances.

In the PS a multitude of particle beams with different characteristics are produced in order to comply with the requirements of the physics users. The previous year (2018) only protons and ions were used in operation for the LHC and other experiments such as: nTOF (Neutron Time of Flight), AD which is a ring decelerating antiprotons which are produced by 26 GeV/c protons hitting a target, the experiments in the East Area of the PS, beams which are provided to the SPS for fixed target experiments. The production of LHC multi-bunch beams is one of the compound tasks PS has to deal with so as to serve LHC physics experiments. To achieve the best performance, PS follows a specific production scheme, where the LHC-type beams transverse emittances should be defined in the PS Booster, whereas the longitudinal structure should be the result of a complicated series of RF gymnastics done in the PS.

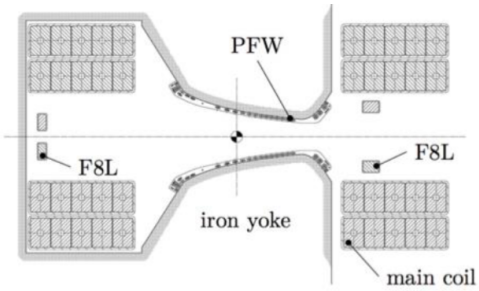

Figure 16: Cross section of the main magnet of the PS. The reference point between the two poles corresponds to the location of the closed orbit. The circuits of the PFW are situated directly on top of the poles. The F8L circuit is located between the main coils as shown above.

PS during operation, needs a special cycle the so called sypercycle, in order to accomodate all types of beam. But at first point, we must explain what a cycle is. A cycle is defined as the sequence of events starting by the ramp of the magnets from 0 current, passing by the injection of the beam, until its extraction to the end-user. As PS is a cycling machine, it can perform a series of these cycles, serving a series of users simultaneously. The unit of time of the cycles is named basic period (BP), which correspond to 1.2 s. The length of a cycle is at least 1 BP and it last several BP.

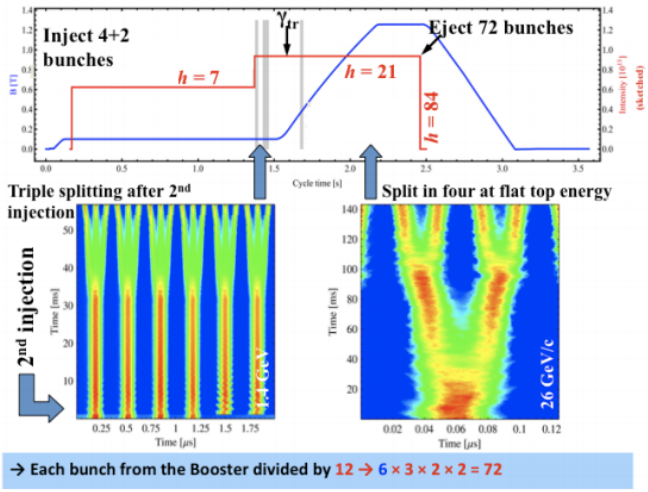

Figure 17: PS magnetic cycle [6]. Injection occurs at 170[ms], transition is crossed at 428[ms] extraction at 835[ms]. Top: The blue curve is the magnetic field as a function of time, ramped up from injection kinetic energy (1.4 GeV) to extraction kinetic energy (26 GeV/c). The red curve is the beam intensity in number of protons and as a function of the harmonic number changed by the RF gymnastics. The RF harmonic is changed from 7 to 21, to 42 and finally to 84, splitting each of the injected bunches in 12. Bottom: longitudinal bunch triple splitting (left) and two double splitting (right)

The LHC beam production requires 3 basic periods of 1.2s each (3 BP = 3.6 s long) to prepare 72 (seventy two) bunches. The first batch contains 4 bunches and the second batch 2 bunches. The bunches are injected from the PS Booster (PSB) at the kinetic energy of 1.4 GeV and accelerated up to a momentum of 26 GeV/c. The first batch is injected at 170 [ms] and the second batch injected at 1370 [ms]. After the injection of the two batches, the beam is accelerated on a second plateau for RF gymnastics. During the second acceleration the PS beam crosses the transition energy around 6 GeV and at top energy the beam is manipulated longitudinally to get the desired bunch spacing before extraction.

An alternative method is the Bunch Compression and Merging Scheme (BCMS) which is characterized by 8 (eight) bunches injected in h=9 on the injection flat bottom plateau, then bunches accelerated on the second (intermediate) plateau to merge in four before triple splitting (10 MHz RF system). Finally, 12 bunches are accelerated on h = 21 (10 MHz RF system) for a final double-double splitting at top energy to get 48 final bunches on h = 84 (20 and 40 MHz systems), then it follows a final bunch rotation (40 and 80 MHz systems).

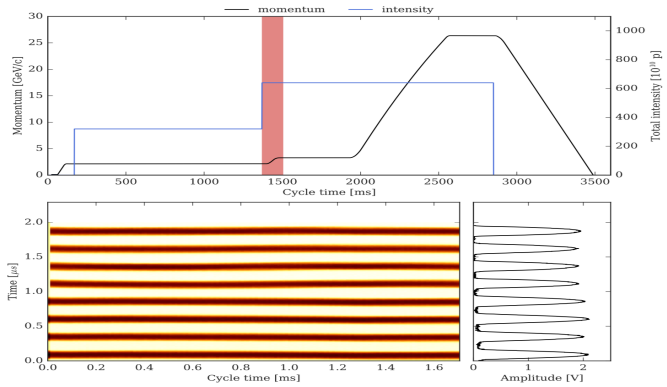

Figure 18: Second injection after 1.2s (waiting time) followed by the acceleration to intermediate plateau: 8 bunches on h = 9 in total.

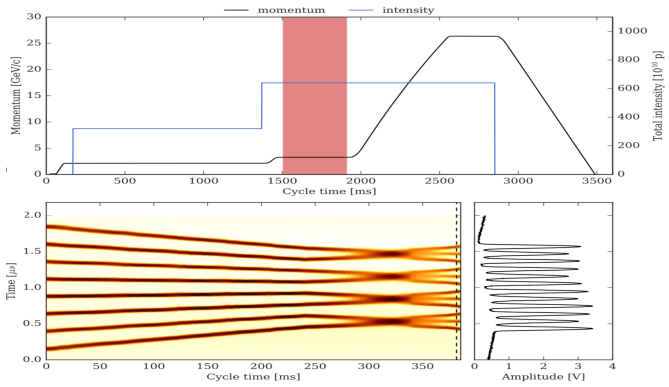

Figure 19: RF gymnastic for the production of the BCMS scheme at intermediate energy. The batch compression is followed by a bunch merging and a triple splitting.

3.2 Beam instrumentation

Beam instrumentation is a key system in an accelerator in order to monitor the operational beams. The beam intensity is one of the most important quantities to monitor, it is measured using beam current transformers (BCT) which infers the beam intensity from the current induced by the passage of the beam inside a dedicated measurement coil. Given its simplicity, the measurement can give the intensity every ms. The beam transverse position is measured using electrostatic pickups (PU).

The transverse tune is measured by a based band tune (BBQ) measurement system, which has been developed at CERN. The measurement of the fractional part of the tune is based on an excitation of the beam and consecutive measurement of the beam response in a fast pick-up over a finite number of turns. The Q-meter software tool in the control room calculates the fractional part of the tunes by Fast Fourier Transform (FFT) analysis of the data.

For emittance measurements the diagnostic tool that is used is a wire which is scanned across the beam very rapidly. Secondary particles generated and then are counted with a scintillation telescope.

3.3 The LHC Injectors Upgrade project

The CERN Proton-Synchrotron is the oldest injector of LHC, and will continue to serve the LHC at least for the next 25 years. In view of this, an upgrade program to increase the luminosity of the LHC by reducing the beam transverse emittance for a larger intensity per bunch has been approved. The LIU project has already begin since 2018 having an ambitious work plan. LIU's target is to double the beam's brightness. According to the technical design report for LIU [3], the injection kinetic energy of the PS will be increased from 1.4 to 2 GeV to mitigate the large direct space charge tune spread of the increased brightness beams which can lead particles to cross many times betatronic resonances. Given the above, the increase of the injection energy to 2 GeV is necessary in order to reduce space-charge-induced transverse emittance blow-up and beam losses.

One major component of the PS that will be also consolidated is the magnet system. As we had already seen in this chapter, proton synchrotron has a total of 100 main magnets within it (plus one reference magnet unit outside the ring). During the last Long Shutdown 1 (LS1) and at the beginning of LS2, a dedicated team performed various tests to identify weak points in the magnets. The data had shown that some magnets needed refurbishment.

Many other experiements will be conducted in order to refine, the meticulous LIU planning process. The measurements that will be introduced in this thesis comprise part of the LIU project.

3.3.1 Motivation Goals and Outline for this thesis

There were several motivations leading to the execution of these measurements. To begin with the production of the LHC beams in the CERN Proton Synchrotron (PS). The long waiting time of of 1.2 s during the 1.4 GeV (kinetic energy) injection flat bottom causes one of the main limitations for high brightness beams, due to the fact that for large betatronic tune-spreads induced by direct space charge, particles can cross resonances many times and finally get lost. Given the above, space charge issues are dominant at injection flat bottom due to storage time of 1.2 s, therefore consequences of this issue like emittance blow-up and beam losses are inevitable. Accordingly, this indicates a need to investigate the different betatronic resonances which exist in the CERN PS at injection energy. Experimental studies at the PS have been performed until the end of the second run in December.

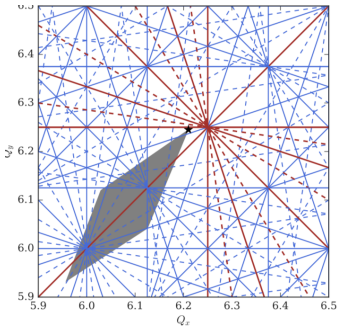

Figure 20: It is observed that there is limited flexibility in choosing the working point.

Additionally, it is well known that PS magnets were installed in the 1950s, and part of these circuits have been added or modified since then, resulting in the fact that dedicated measurements on the resonances were mandatory. Measurements of this kind had been performed again in 2012 and have shown that several effects, such as the alignment of the main magnets, can affect the resonance strength. Repetition of these measurements will give in detail information about the magnetic stability of the machine thus will clarify possible changes in resonance strength over time. It has also observed that different remnant magnetic fields which appear in some non-linear circuits such as sextupoles and octupoles, have a great impact on the resonances. So this project intends to determine the extent to which such remnant magnetic fields affect the resonances.

The thesis aims also to focus on the investigation of the resonances which stem from the non-linear magnets used for the MTE Extraction. A new extraction technique, the Multi-Turn Extraction (MTE) has become operational in September 2015. MTE relies on the application of non-linear magnetic fields, and higher order resonances might therefore be excited by remnant fields.

Last but not least, the Low Energy Quadrupoles (LEQ), which are used to control the tunes, have received new power converters, allowing us now to explore a larger extent of the tune diagram.

Collectively, these studies outline a critical role for the knowledge of the existing resonanses in the PS. Qualitative and quantitative research had done in order to provide with the results.

4 Tune diagrams at 1.4 GeV

The major objective of these studies was to investigate the impact of resonances along the PS. Particles are led to resonant conditions due to the presence of remnant magnetic fields, in the machine. These remnant fields stem from different circuits as sextupoles, octupoles or PFW, which are non-linear magnets who excite different kind of resonances. As it was mentioned in a previous chapter, some these dedicated non-linear magnetic circuits are consecutively used for different operational reasons (eg. MTE.). Apparently, a necessary use of these circuits leads PS magnets to accommodate couple of remnant fields. This indicates a need to understand the magnetic effect of these circuits. Studies performed in 2018 seek to obtain data which will address and evaluate the resonance excitation due to the remnant magnetic fields of non-linear circuits.

Apart from the previously illustrated reasons, these studies make a great contribution to examine the magnetic stability of the machine, since alignments of the main magnets have taken place through years and therefore led to possible magnetic misalignments.

Overall, resonances' behaviour might be affected given the previous reasons. In this chapter it will be discussed and examined the results of this campaign. Data of these measurements carried out in 2018 and derived from dedicated machine development (MD) studies.

4.1 Measurements performed in 2012

Preliminary work in this field focused on the future injection energy of 2 GeV. There where couple of reasons, that had been led measurements to inevitable exploit PFW for the control of the working point. As we had seen in a previous chapter, there are some extra magnetic elements, the so called Pole Face Windings (PFW), have been mounted to the main magnets. These elements, used for the chromaticity correction at the low energy by 2012. Back then they only used at high energy for chromaticity control. So, in order to examine the influence of PFW on the machine resonances, dedicated measurements at low energy should have been conducted during 2012. Additionally, tune variation performed exclusively with PFW due to the insufficient strength of the LEQ to achieve -the desirable for the measurements- 2[GeV] energy. In general LEQ used to control the transverse tunes, as done in the measurements conducted in 2018. However, it is clear that the main focus was on measurements at the LIU injection energy at 2[GeV]. Then, PFW are nowadays used for chromaticity correction at low energy, so a deduction about their impact on resonances had been considered to be necessary.

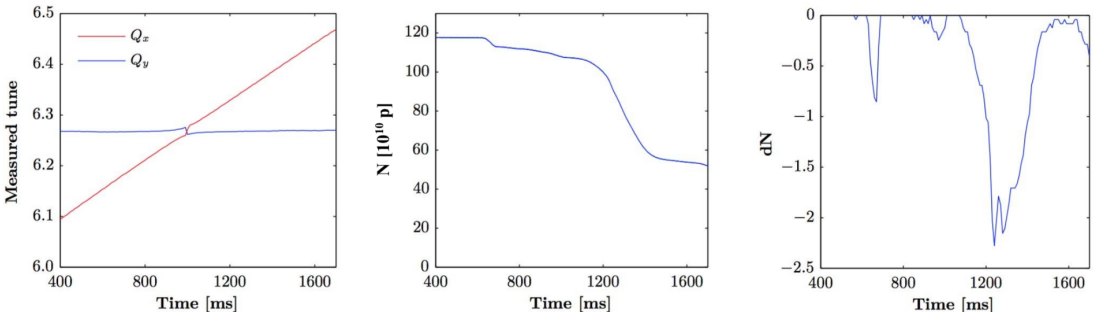

Figure 21: In a previous study done [1] experiments were carried out using the conditions described below.

Measurement procedure had been done at the CERN Control Center, using a beam of a large emittance. In order to acquire the desirable data, a particular procedure had been followed. During one cycle period, tune in one plane kept constant, while in the other plane was dynamically changed. Before recording both tunes and intensity, a global correction of linear coupling was done. Finally, inference of information about resonances, came from the derivative curve of the intensity signal.

These studies had reached the conclusion that , the regime around operational working point (6.2,6.4) is rather resonance free. Also, there had been observed very strong normal and skew sextupole resonances, but no resonances above 3rd order.

The choice of working point appeared to be constrained by two resonances, the vertical integer $Q_y = 6.0$ and the vertical third order $3Q_y = 19$. Subsequent studies revealed additional resonance at $4Q_y = 25$. It is actually the space charge driven structural resonance $8Q_y = 50$.

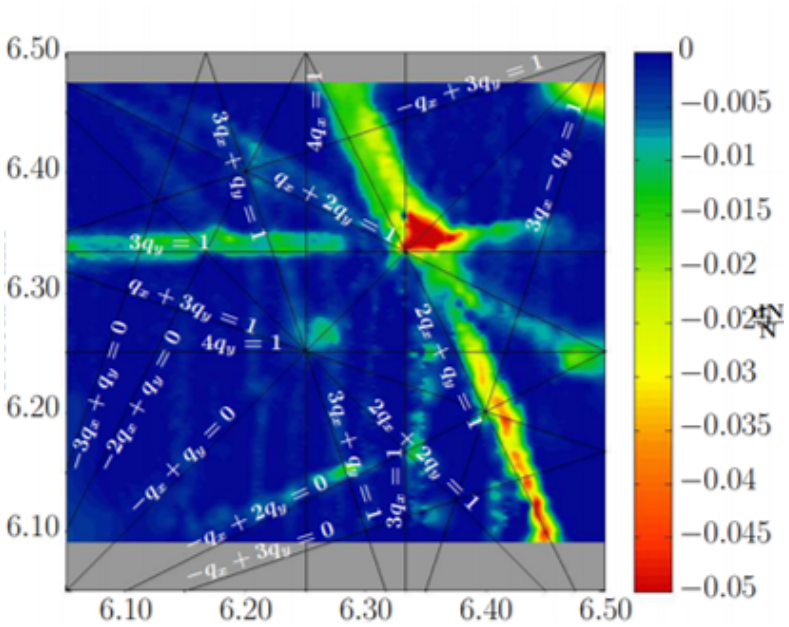

Figure 22: Tune diagram. Depicted resonances concern order up to 4th. Courtesy of Alexander Huschauer.

Parameters	2012
Kinetic energy [GeV]	2
Harmonic number	8
Number of bunches	1
Number of protons per bunch [10^{10}]	120
Bunch length (4σ) [ns]	117
Relative momentum error (1σ) [10^{-3}]	0.8
Longitudinal emittance (matched area) [eVs]	0.84
Normalized horizontal emittance (1σ) [mm mrad]	10.4
Normalized vertical emittance (1σ) [mm mrad]	7.64
Horizontal direct space charge tune spread	0.05
Vertical direct space charge tune spread	0.06

Figure 23: Beam and machine parameters of measurements performed in 2012.

4.2 Dynamic scans performed in 2018

Due to practical constraints measurements performed in 2012 restricted to use exclusively PFW for tune control. That was a considerable limitation for the measurements back then. Nowadays, LEQ have received new power converters, allowing studies to explore a larger extend of the tune diagram. Accordingly, there was the possibility to use LEQ to assess the existing resonances in the PS. Therefore, dedicated tune scans were performed to investigate resonances around a certain region and especially examine the area around the working point. Tune diagrams measurements is a major project of interest as the selection of the operational working point depends on the loss map analysis. Thus selection of the WP should be accurate so as to be in a resonance free area.

Parameters	2018	2012
Kinetic energy [GeV]	1.4	2
Harmonic number	8	8
Number of bunches	1	1
Number of protons per bunch [10^{10}]	100	120
Bunch length (4σ) [ns]	160	117
Relative momentum error (1σ) [10^{-3}]	0.99	0.80
Longitudinal emittance (matched area) [eVs]	1.24	0.84
Normalized horizontal emittance (1σ) [mm mrad]	11.8	10.4
Normalized vertical emittance (1σ) [mm mrad]	7.14	7.64
Horizontal direct space charge tune spread	0.04	0.05
Vertical direct space charge tune spread	0.06	0.06

Figure 24: Beam and machine parameters of measurements performed in 2018.

4.2.1 Measurement principle

In order to know the effective resonance lines in the machine, a series of tune scans had been performed during 2018. Again the experimental set up had been done at the CERN Control Center, using a beam of a large emittance. For the systematic tune scans a dedicated machine development (MD) PS cycle was used. The beam was prepared and injected directly to PS from one of the four rings of the PSB. Then beam conditions were measured at the injection plateau (1.4 GeV). In order to perform our measurements, the beam is kept at the injection plateau for 2.4 s (=2×basic period=1.2s)

Tune scans were programmed using dedicated Matlab scripts. Specific devices were manipulated through a special framework called JAPC (Java API for Parameter Control), which is part of the accelerator control system and allows to communicate with the various devices installed in the machine. The scripts had been adjusted depending on the desired configuration. For the tune measurements a software tool in the control room called Q-meter was used. Through this device both vertical and horizontal tunes were measured depending the selected configuration. During this experiment, the PS's Low Energy Quadrupoles currents were continuously adjusted, in order to change the horizontal and the vertical tune along the cycle. The transverse tunes were adjusted before the beam was injected. Before starting to save the data, it was necessary to correct the closed orbit distortion (COD) in the machine. The COD is the deviation of the particles trajectory from the design orbit and is generally excited by dipoles errors and quadrupoles misalignments. Without COD correction, it was impossible to obtain good measurements due to the huge losses. Once corrected the COD, instead, it had been possible to retrieve accurate information about tunes and intensity. Finally, data were recorded on a database and afterwards post-processing was done through Python scripts.

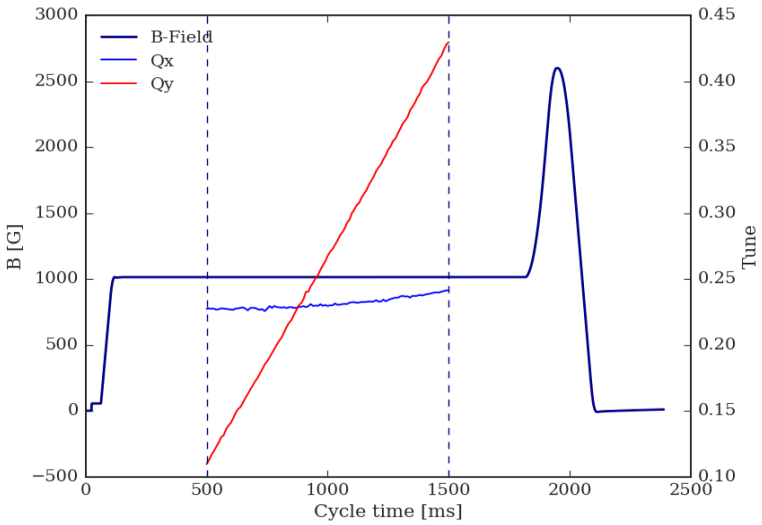

Figure 25: Measured magnetic field along the PS, together with the measured tunes,horizontal and vertical.

In this investigation there were several sources by which several error values had been occurred. As anticipated, there were some plausible problems due to the multiple PS users. One of the main problems was that another user's beam might had affected our beam's characteristics.

So, for this reason, our operational beam had been always placed in front of a zero cycle, so as not be affected. It was a functional way, to guarantee the relative beam losses remain well below 2% and at the end the beam injected in the PS from PSB conserve the maximum intensity possible. There was also the extreme possibility that a different user might had unconsciously altered beam's characteristics. Another, obstacle was the bounded offered time for collecting our data, which led to gather a restricted number of data for statistics. Hence, the number of repetitions was confined, from five repetitions to three of the same scheme each time. The cases presented above, illustrate the difficulty of collecting data. Consequently, the aforementioned problems share an important premise: the creation of a good filtering Py-script prepared in accordance with beam's characteristics. Although, the performance was demonstrated far from smooth, the conclusion was to collect considerable data, which had yielded significant results.

The procedure continious following the steps outlined below. At first point, a bunch with large transverse emittances was injected from PSB. The criteria for selecting such a big beam's size is firstly because the direct space charge tune spread should be reduced thus such a beam size would eliminate it. Then, it would be important for our results to make the beam fill the whole vacuum chamber and be sensitive to losses during resonance crossing. As for the next step, the bunch was kept on a flat bottom (1.4 GeV) between 500 and 1500 [ms] (= 1 s). Presented data afterwards, concern measurements during this time. Then, during one cycle, tune in one plane was kept constant, while in the other plane was dynamically changed. At the next cycle, the constant tune will be increased by a predefined step, while tune in the other plane will remain the same until constant tune reaches a specific margin. This boundary came from the limitation of LEQ to reach more area above thus defined the area of the tune diagram. To reduce the risk of coupling between the planes, Q_h,Q_v were excited and measured on separate cycles, while the intensity was recorded only when the tune was not excited. Ultimately, information about resonances came from the derivative of the intensity curve witch is derieved out of the BCT signal. Normalized derivative values were calculated and then plotted for the reproduction of the tune diagram. Derivative values were normalized with the the intensity value prior to each resonance crossing.

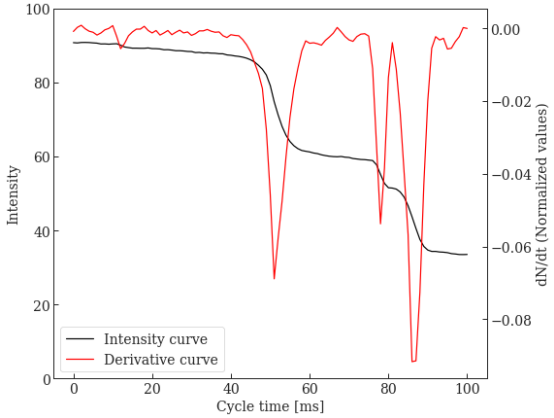

Figure 26: Intensity curve, with its derivative curve when tune in the vertical plane kept constant, at the previous cycle, at $Q_y = 6.24$. Reasonances were identified by beam losses.

4.2.2 Emittance measurements

Measurements of this study, had been excecuted during the last run period, starting from May until the middle of November. Accordingly, considerable attention had been given to preserve the transverse emittances constant, along this period of time. In a different case, results of the acquired data would have not been correspond to the same beam's characteristics. Thus, the combination of the data would not be accurate. Consequently, it would not be prudent to draw conclusions about the outcome of results. Given the above, there was a demand at PSB oparators to measure the transverse profiles three different times during these months of measurements. This procedure had been done using a wire-scanner, which averages the beam profile during about a thousand turns.

Interestingly, these tests showed that no significant difference was identified between beam sizes. It can be concluded that, emittance changes were negligible.

XL_EMIT	12.07.2018	02.10.2018	*DIFFERENCE*
From R3:	MEASURED	MEASURED	*/Dx/x [%]*
Dp/p[E-3]	0.87	0.99	12.90
El[eVs]	1.24	1.12	10.16
Bl[ns]	181.0	163.0	10.46
Int[E10p]	105.1	99.9	5.07
Eh[1on]	11.98 (0.32)	12.08 (0.38)	0.83
Ev[1on]	7.14 (0.25)	7.66 (0.02)	7.02
Bright[-]	11.0	10.1	8.53

Figure 27: Beam's parameteres measured at PSB.

One additional measurement had been done for accuracy reasons.

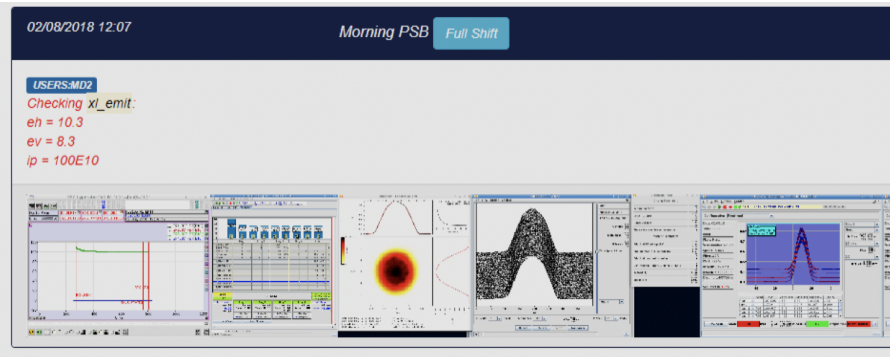

Figure 28: This is a picture from the apparatus of PSB used for emmitance measurements, in the control center.

4.2.3 Tune diagrams for standard configuration

With the execution and completion of our experimental set up, the first set of data was gathered. In order to reliably produce the tune diagrams, measurements replicated five times. The theoretical tune diagram contains the resonance lines up to fourth order, where the solid lines indicate regular and the dashed lines skew resonances. Superimposed tune diagram, illustrates the one generated by the measured points. Tune variation controlled only with LEQ, and due to their currents' limitation, measurements were restricted in a specific area (Q_x, Q_y varies from 6.10-6.40).

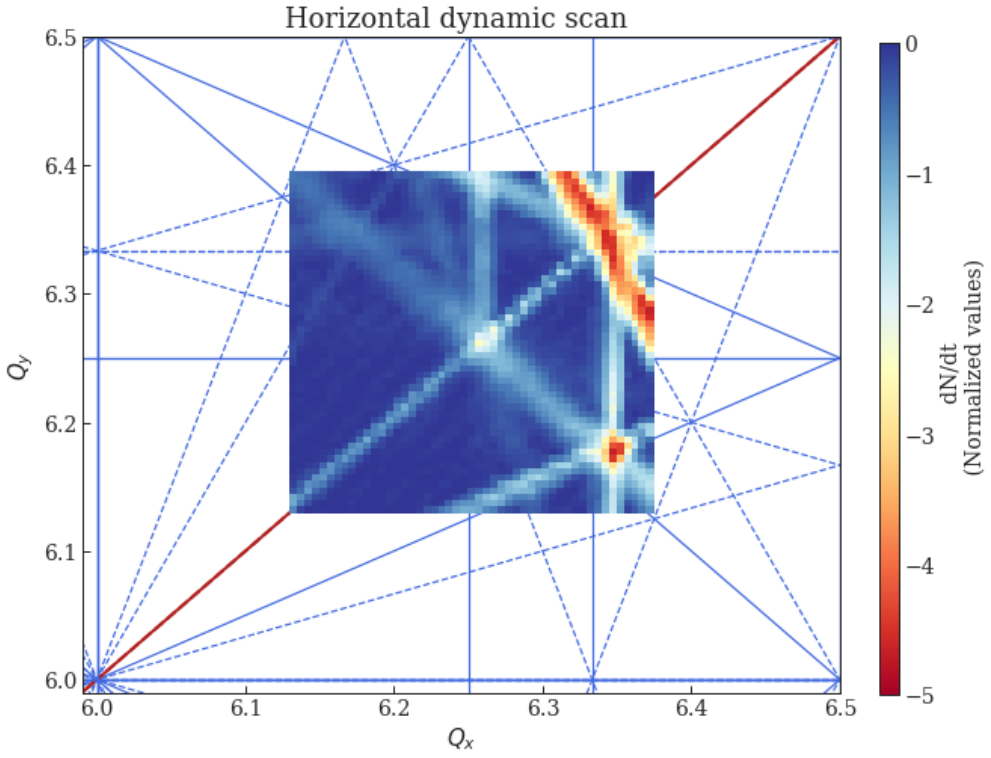

Figure 29: Tune diagram of a horizontal dynamic scans.

The loss map depicted in the diagram above derived out of one of the very first measurements that had been done and consists the outcome of two tune diagrams of different configurations superimposed. The first configuration was a tune scan where the tune in the horizontal plane was dynamically changed (from smaller to larger tunes) while the tune in the vertical plane kept constant and augmented by a constant step of 0.01 after each cycle. The second prepared configuration was in compliance with the previous one, but the tune in the horizontal plane was dynamically changed from larger to smaller tunes. The final resulting tune diagram contained the mean values of the two cases described above.

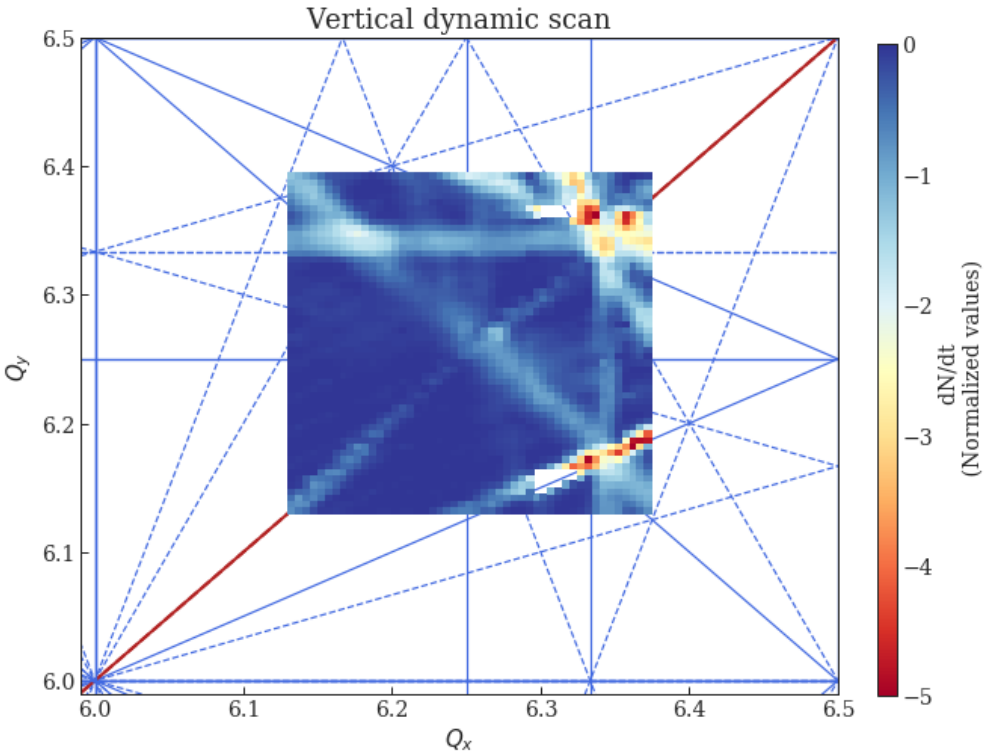

Figure 30: Tune diagram of a vertical dynamic scans.

As soon as, the horizontal dynamic scan measurements and post processing had finished, the vertical dynamic scans launched. This experimental procedure followed the same steps as the previous set up, having now the dynamic scan conducted in the vertical plane. The final diagram of the gathered data is represented above.

To assess the resonant conditions carefully, a tune diagram more detailed would be necessary. Loss map in this case would contain all the resonant lines created out of the measurement values. On these grounds, the generation of such a tune diagram followed, its points derived from scans in all directions described above. As soon as these steps have been carried out, we were now ready to plot the values to combine measurement results.

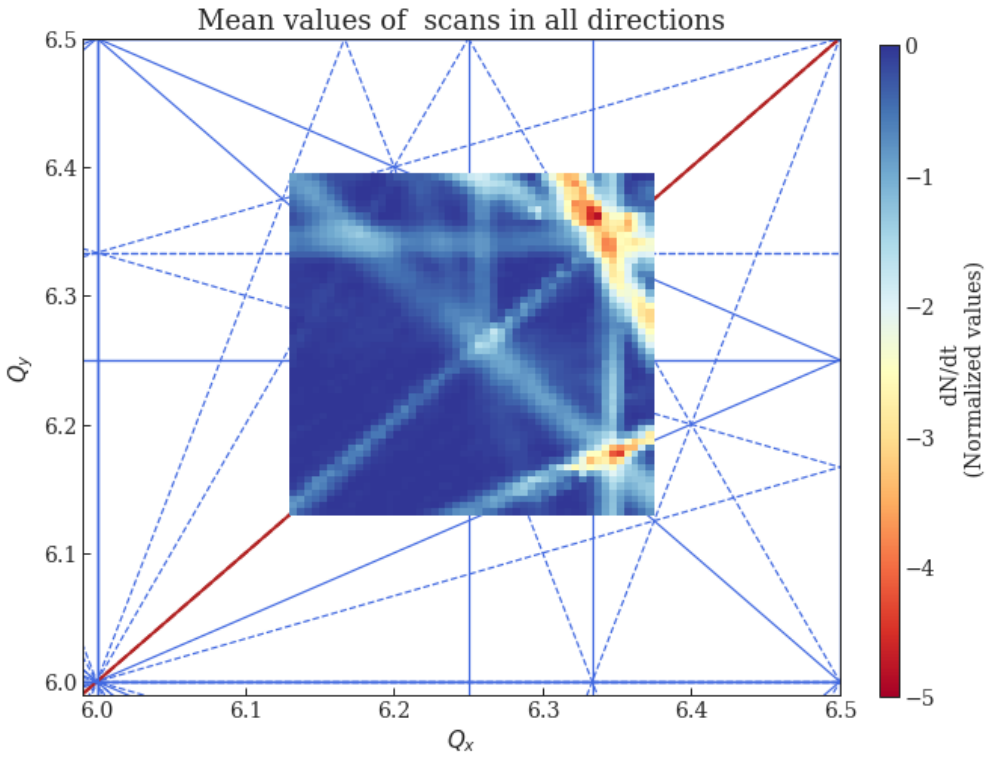

Figure 31: The illustrated tune diagram, was generated out of the mean values of all configurations, both horizontal and vertical scans, in all directions.

In view of all that has been mentioned so far, one could deduce that the loss map analysis plays an important role also in the choice of the working point. As we had see in a previous chapter this point denotes the area in the tune diagram Q_x, Q_y the machine is designed for. The choice for the working point is determined by resonance stop-bands in the tune diagram. Regarding the stop-bands, they are generated from tune shift, which space charge forces provoke. Space charge is the ingredient to amplify the resonance excitation, as well as to shift the betatron resonance condition to the higher value. Space charge forces can excite third and fourth order resonances. We can examine this hypothesis by comparing the theoretical lines with the ones originated from measurements. It is easily observed that resonant lines differ from the theoretical ones' in width and placement. The above experimental loss maps confirm the presence of space charge induced tune shift.

Additionally, the first set of data highlighted the impact of remnant fields, came from non-linear elements, to resonances. Forth and third order resonances observed very clearly compared to the past. Given that sextupoles build the major part of nonlinear elements in the lattice due to the chromaticity correction scheme, the presence of third order resonances is inevitable. For instance, they could possibly stem from non-linear fields used for MTE (since 2015). Further, remnant fields in PS, were generated by other beam cycles and possible had amplified the resonant conditions.

4.2.4 Tune diagrams for low chromaticity configuration

One of the major limitations for operational beams is chromaticity, which its presence might be lethal for the beam itself. Since 2012 PFW were used at low energy to control chromaticity while in 2018 there was the idea to exploit some dedicated sextupoles instead. The premise to execute this concept is to be aware of the possible resonances that the specific circuits might excite. Accordingly, further research on these configurations about resonant conditions was necessary.

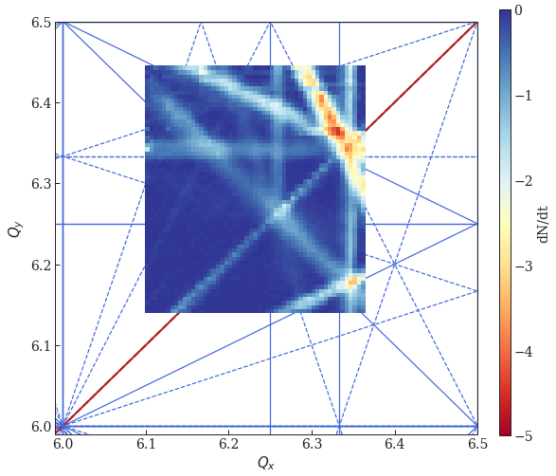

Figure 32: Tune diagram for standard configuration.

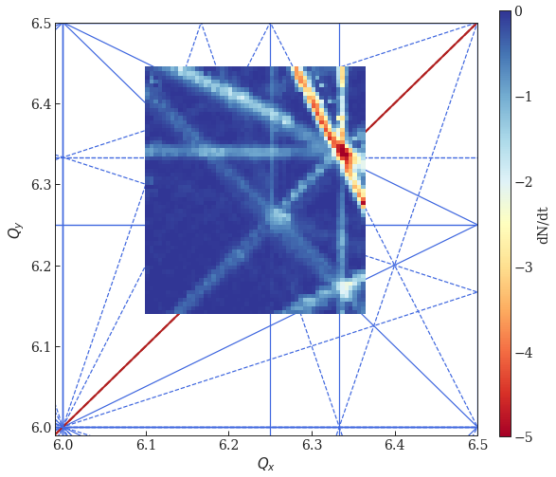

Figure 33: Tune diagram for BCMS low-chromaticity configuration.

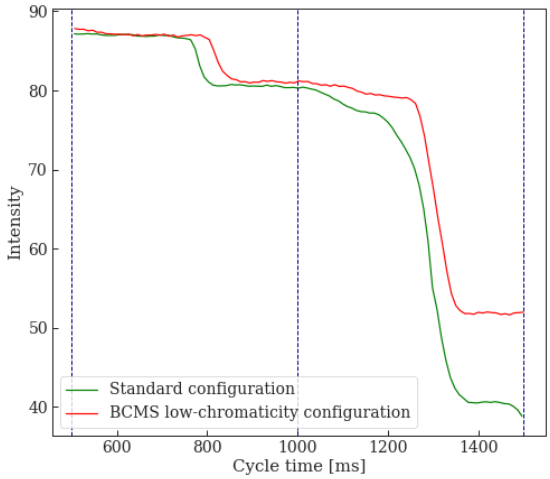

Figure 34: BCT signal for a fixed vertical tune of 6.18, at standard configuration.

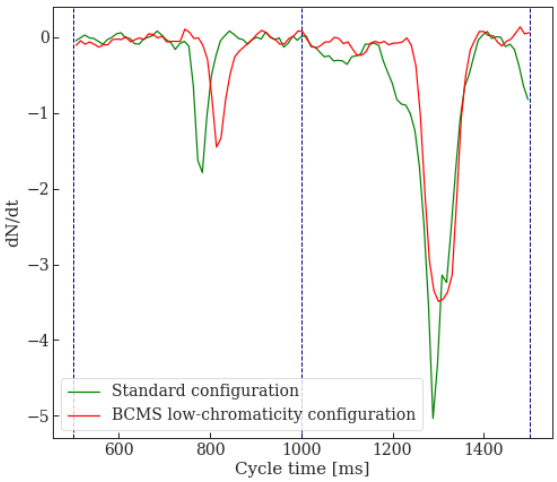

Figure 35: Derivative of the BCT signal for a fixed vertical tune of 6.18, at BCMS low-chromaticity configuration.

To perform measurements for BCMS low-chromaticity configuration, PFW circuits had to enabled in our MD cycle. For this procedure PFW currents were selected from flat bottom of the ones of the BCMS cycle. Then, dynamic scans had been released, to verify if no other resonances were excited in this case. In the initial stage of the process PFW were disabled for the scans, which were conducted again in four different directions. The next set of scans followed the same way, but now PFW were enabled in our beam cycle. The scans concerning the standard configuration scheme, they should had been repeated in this set of measurements, because their time of execution precede the previous ones couple of moths.

That means, there was a need firstly to verify if resonances behaviour had changed over time, plus to compare the two cases in the same time lapse. Finally, after data analysis we observe the tune diagrams above. (each generated out of the mean values of the four directions.)

Concerning the first two diagrams figure: 34,35, it is identified a significant difference between the resonant lines. They are clearly smaller in width in BCMS low-chromaticity configuration. Therefore, losses seem to be less in that case. This suggests a further analysis in the intensity curves. Looking the intensity curves and the derivative ones figure: 36,37 respectively, it is confirmed that less losses occur when PFW are enabled for chromaticity correction.

These tests interestingly showed that, no additional resonances had been excited. (in contrast to chromaticity correction with dedicated sextupoles) The post processing revealed very interesting results making so far PFW a good candidate, for chromaticity correction.

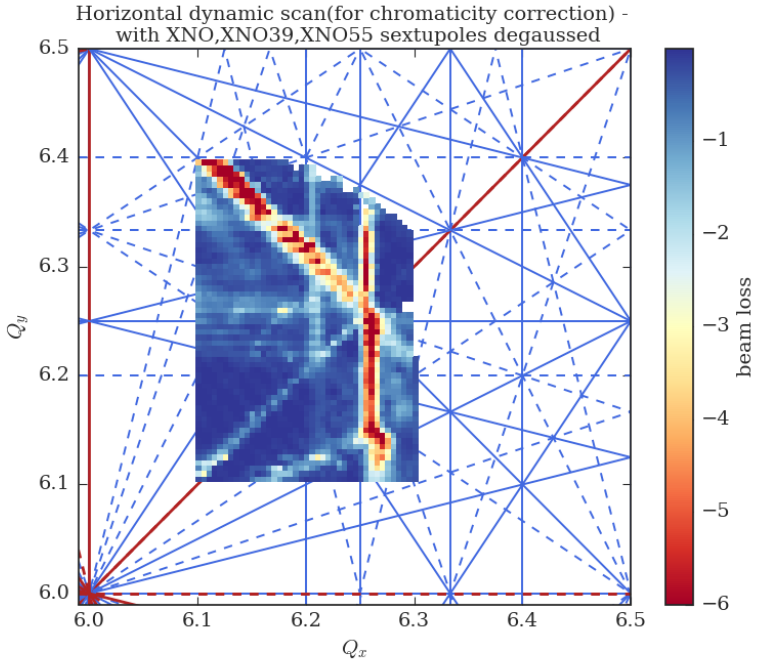

Figure 36: Tune diagram for the new chromaticity correction scheme.

Now let us turn our attention to the the new scheme results. Regarding the new low-chromaticity configuration, sextupoles used for MTE, and some new vertical sextupoles required to be enabled in our beam cycle. To assess the new scheme, loss map analysis was used to predict possible excitation in resonances. White areas correspond to missing data due to very low beam intensity. While we observe that only a restricted area in the tune diagram could be generated. This underlines just how strong the $4Q_x = 1$, $2Q_x + 2Q_y = 1$ resonanses proved to be. In other words, the sextupoles enabled in our cycle, excited so strong the fore-mentioned resonances that no intensity left in the beam to further extend the tune diagram. Hence, the alternative solution to use dedicated sextupoles proved to be inappropriate for operational utility.

4.3 Static scan at 1.4 GeV

It has been observed from the previous scans that different kind of resonances PS accomodate. Because of the importance of some resonances, it was intensively studied through static scans their existence.

Static scan forms an alternative solution for resonance investigation, though slightly more complicated and time-consuming. So, as we where interested for specific resonances static scans conducted in a restricted area, because of restricted time. The difference between dynamic and static scan concerns the way tune is measured. In a static scan both horizontal and vertical tunes were kept constant. Each time one plane kept constant while the other was shifted by a specific step with respect to the other plane, until a predefined boundary. In that way the area was completely scanned, which means that the gathered data would provide us all the information about the presence of resonances.

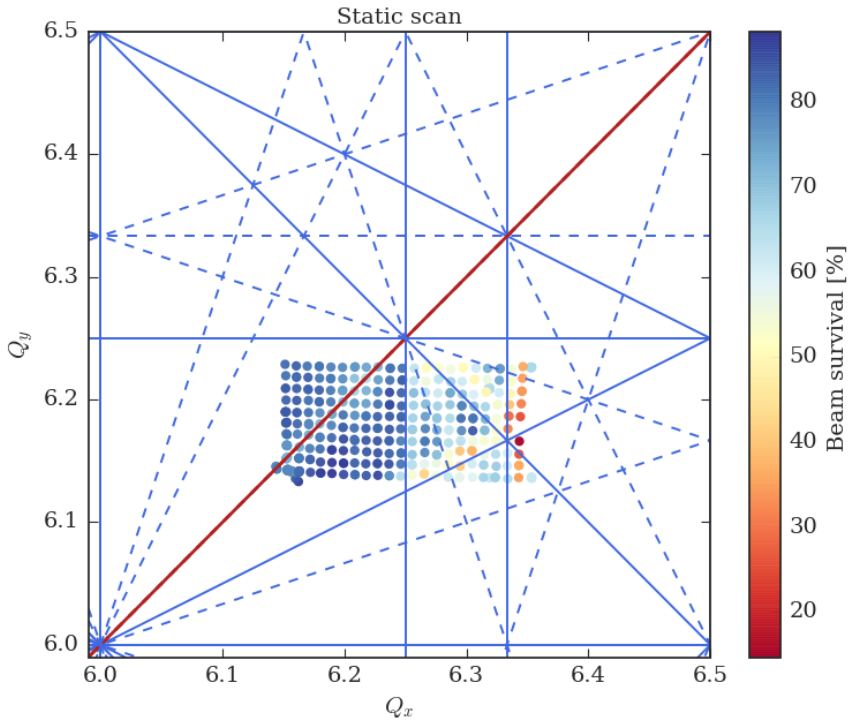

Figure 37: Static scan in a determined tune area ($Q_x : 6.13 - 6.22$, $Q_y : 6.13 - 6.25$).

All samples were thoroughly checked for the data analysis. To represent the strength of each resonance, the percentage of the beam left was calculated and then plotted. So far we have observed from dynamic scans the resonances: $3Q_y = 16$, $2Q_x + 2Q_y = 1$, $4Q_x = 1$, $-Q_x + 2Q_y = 0$, $-Q_x + Q_y = 0$. Studies on static scans confirmed their existence.

4.4 Important remarks

Overall, this project provided an important opportunity to advance the understanding of changes in resonance excitation over time. Tune diagram measurements revealed very different resonance excitation with respect to 2012. Loss maps obtained from scans in four different directions, demonstrated resonances up to 4th order. Remnant fields, could well be responsible for these resonances. Could possibly stem from non-linear magnetic fields used for MTE.

Further data collection were required to determine exactly the presence of $3Q_y = 16$, $2Q_x + 2Q_y = 1$, $4Q_x = 1$, $-Q_x + 2Q_y = 0$, $-Q_x + Q_y = 0$ resonances. Ultimately, static scans confirmed their existence.

There was a positive suggestion, to use MTE sextupoles and some new vertical sextupoles instead of PFW, for chromaticity correction at injection energy. These findings, great impact on resonance excitation investigated with tune diagram measurements.

Experimentally tested, through dynamic scans that chromaticity correction with dedicated sextupoles instead of PFW strongly excites additional resonances. As can be seen, these sextupoles cannot be used for operation as they excite too strong resonances.

All in all, we indeed see a qualitative difference in the resonance excitation by observing the tune diagrams. Given the above, it can be also concluded, that PFW occur to be a good candidate for chromaticity correction.

5 Investigating the existence and effects of remnant fields in PS

The CERN Proton Synchrotron (PS) provides different types of beams at different extraction energies. The magnets (main magnets, multipoles, etc) of the PS are regulated with a current loop. Due to their magnetic properties they introduce the hysteresis effects in the PS, hence that indicates a major limitation on efficiency and operation of the beams. The aim of our research was to further broaden current knowledge of resonances behaviour. To do this, it was necessary to eliminated all the possible remnant effects that some special multipoles had accommodated. This chapter summarises the measurement procedure of this study, and also the results of the gathered data.

5.1 Remnant magnetic effects of octupoles, sextupoles

When an external magnetic field is applied to a ferromagnetic material (like the material of some dedicated multipoles of PS), the atomic domains align themselves with the field. Even after the elimination of the field, part of the alignment will be retained. As a consequence, the material has become magnetized. To demagnetize it requires, a magnetic field in the opposite direction.

Magnetic Hysteresis can be defined as the way a material's magnetic properties lag behind the force that creates those properties. The hysteresis curve tells us a lot about a material's response to a magnetic field. We plot a material's hysteresis on a graph known as the Hysteresis Loop (see Fig. 40), which also can be defined as the relationship between the external magnetizing force and the induced magnetic flux density. In the presence of a magnetic field, the Flux Density (B) of a magnetic material will increase, until it reaches a maximum value where it no longer responds to increases in the magnetic field. This is the point of saturation.

Remanence is the remaining magnetic field found in the material after the applied magnetic field is reduced to zero. The amount of (H) required to drive (B) to the zero line gives us a value for the material's Coercivity.

Imperfections in the magnetic field in alliance with the remanence can inevitable lead to resonant conditions thus introduce emittance growth which may result to severe beam losses. Uncertainties on the magnetic field in the PS magnets may originate from non-uniformly distributed material properties.

Experiments on demagnetization of some dedicated multipoles were carried out, in 2018 in order to better investigate the tune diagram resonant lines. Especially, remnant fields in octupoles and sextupoles used for MTE appeared a good candidate to explain the additional horizontal resonances. Therefore, it was of a great importance to identify the origin of each resonance through this procedure. This study will be dealt with in more detail in this section.

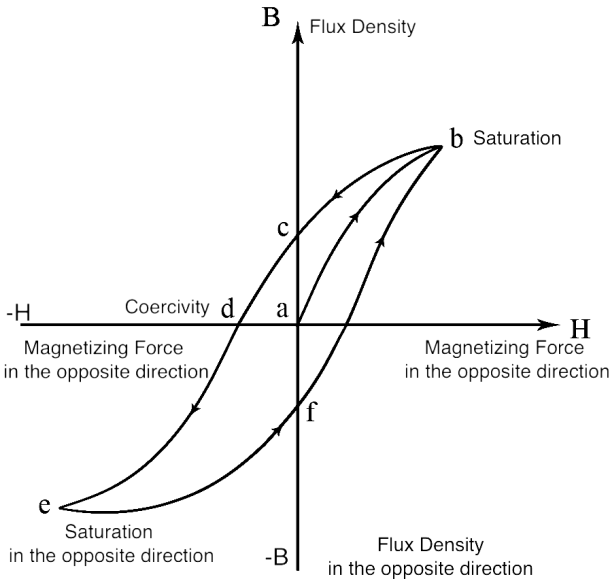

Figure 38: B-H Curve of Magnetic Material. As we follow the letters from a through h we generate important magnetic data about the material response to an external magnetic field. Due to Remanence, we will never get back to point a where we started, because point a was the point where the material had never been exposed to a magnetic field.

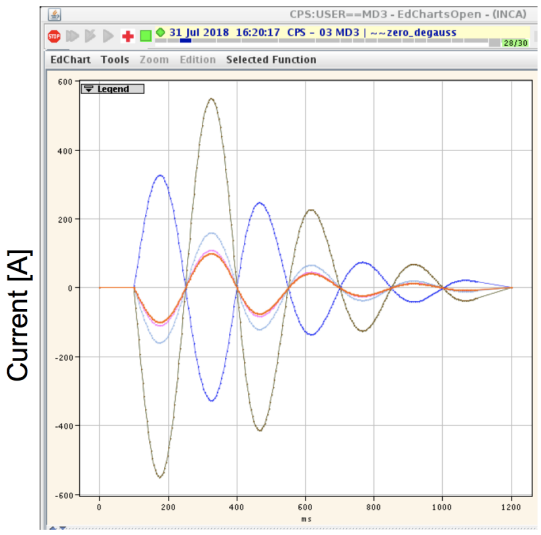

Figure 39: Degaussing programmed fuctions of octupoles (PR.ODN, PR.ONO39, PR.ONO55) and sextupoles (PR.XNO39, PR.XNO55, PR.XNO).

5.1.1 Dealing with the remanence

An experimental study was carried out to extensively explore the impact of the remnant fields in the resonance excitation. Preliminary work in this research focused primarily on the control of the currents of the multipoles which were selected to be used for investigation. In operation, in order to demagnetize the multipoles we followed the degaussing technique. To degauss the circuits entails the excitation of the multipoles with plus/minus the operationally used maximum current followed by an amplitude decay. The currents' set up had been applied in the control room through a specific apparatus of the PS control system. One could see the applied functions in Figure 39. This technique was applied in a zero cycle in front of the MD cycle, on which the circuits were degaussed.

To collect the data, firstly launched a measurement of tunes and intesnsity with the degaussed circuits and then followed a measurement without degaussing them, so that we could guarantee the accuracy of the comparison between the two cases. Observed results will be demonstrated in the following section.

5.1.2 Impact of degaussing on resonances

Much attention has been drawn to the remnant fields of specific octupoles and sextupoles, as they were used for MTE thus appeared to be a good candidate to explain the additional horizontal resonances.

The working point has been raised above the $Q_y = 6.39$ and the measurement procedure is based on the previous one. In the case where the circuits did not get degaussed we clearly observe the same resonant scheme as in the prior set up. The resonant scenario changes in presence of the zero cycle in front of the MD cycle.

The first set of analysis highlighted the impact of degaussing on the resonances (see Figure 40). A striking feature of the loss pattern is been manifested after the degaussing of octupoles and sexpupoles together. In Figure 40 the right diagram represents the case in which we did not degause the multipoles, while the right one introduces the case when we degauss the circuits. The derivatives of intensity now are normalized to prior of the intensity value in order to clearly extract information about the actual loss rate of the beam left each time.

The data yielded by this study convincing evidence that some resonaces clearly disappeared and some others were reduced in strength, leading to less non-linearities in the machine. A closer look at the diagrams indicates that the third order resonance $3Q_x = 19$ is totaly eliminated after the degaussing. At the same time fourth order resonances seem to be reduced in strength, like the $4Q_x = 1$.

At this point little is known about which kind of multipole had an important impact of degaussing on the resonances. To clarify this hypothesis there had been launched a measurement in which the degaussing had done only in octupoles. In that way we would be able to compare the case when the octupoles were degaussed with the case when all the circuits were degaussed. Overall, no significant difference perceived between the two cases. By looking carefully the Figure 42 one could deduce that there is no important impact of sextupoles in degaussing. This was somehow expected, as sextupoles are operated far from saturation regimes. Finally, we have proven that octupoles seem to be main contributors to the resonances.

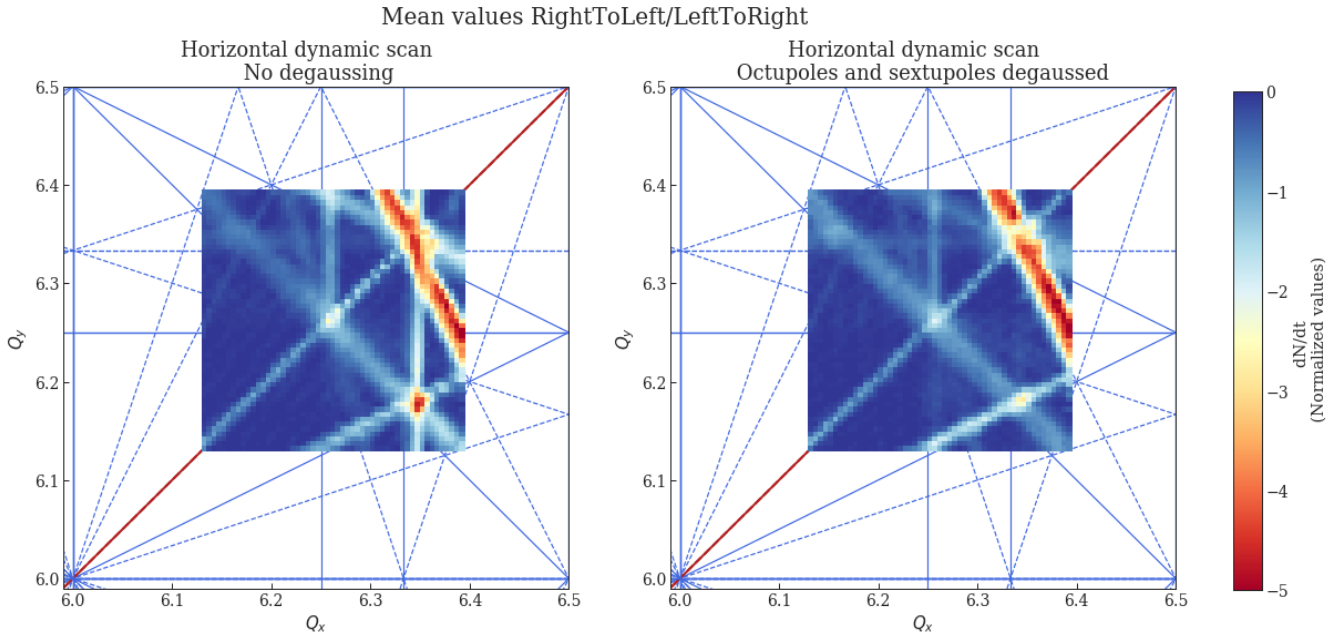

Figure 40: Left tune diagram is generated without degaussing any circuit, while its values are derieved from the mean values of horizontal scans in the two directions, on the other hand the right one represents the case after the degaussing of octupoles and sectupoles.

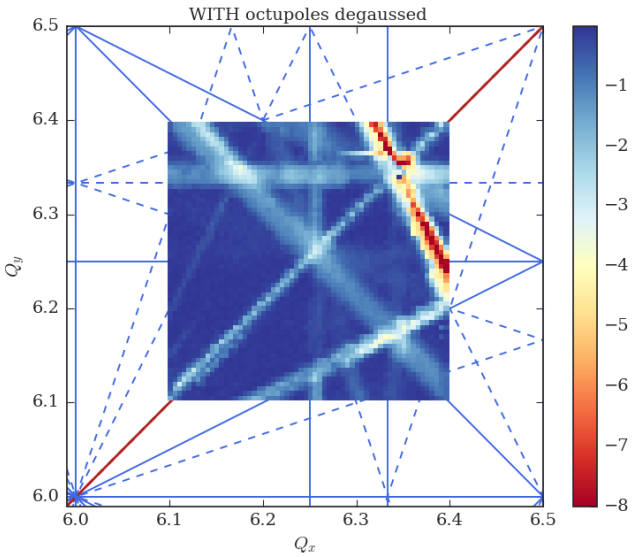

Figure 41: Tune diagrams with degaussing only the octupoles.

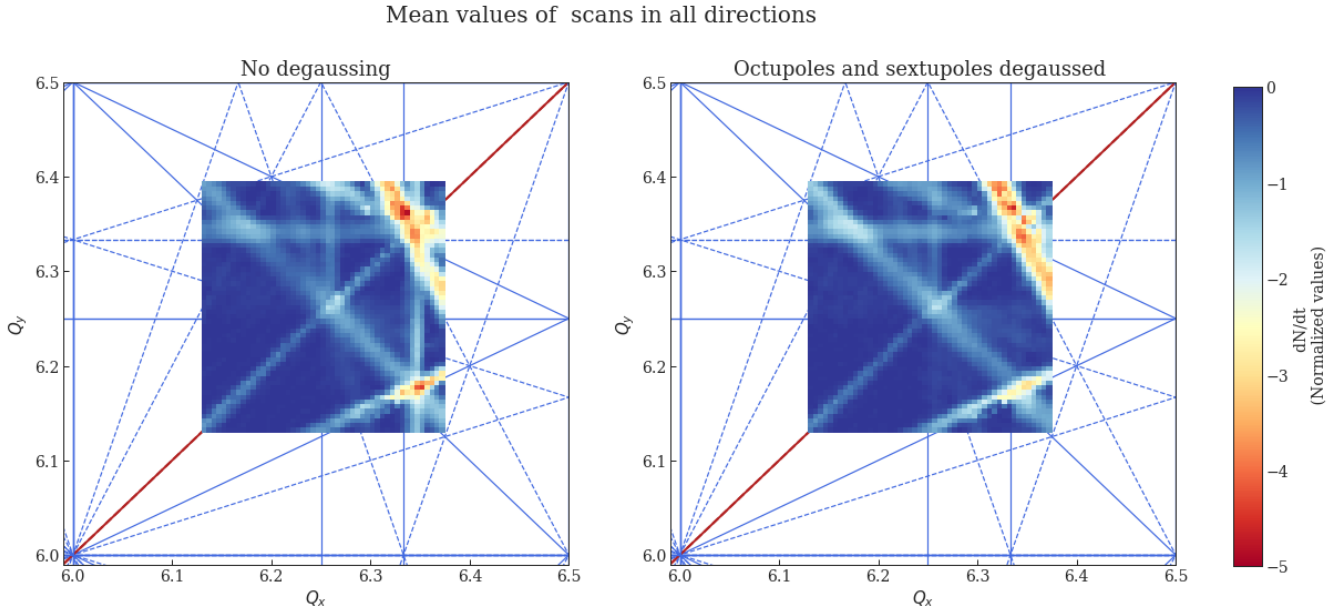

Figure 42: Left tune diagram is generated without degaussing any circuit, while its values are derieved from the mean values of dynamic scans in the four different directions, on the other hand the right one represents the case after the degaussing of octupoles and sectupoles.

The tune diagrams depicted in figure 43, describe the two cases when there is implemented or not the degaussing in the multipoles. The represented values are originated from loss rate of each corresponding point in the diagram. Each of the two diagrams was generated from the mean values of derivates of the four different directions.

Our findings would seem to outline the great impact degaussing has in the resonance excitation. For this reason there had been an important need of meticulously explore the amplitude and FWHM the of each resonance. One notes that even from a horizontal scan (figure 44) we could derive a lot of information about the resonance behaviour before and after the degaussing. Further studies through data analysis focus on finding clear evidence of how the resonances of a horizontal dynamic scan are influenced after the degaussing.

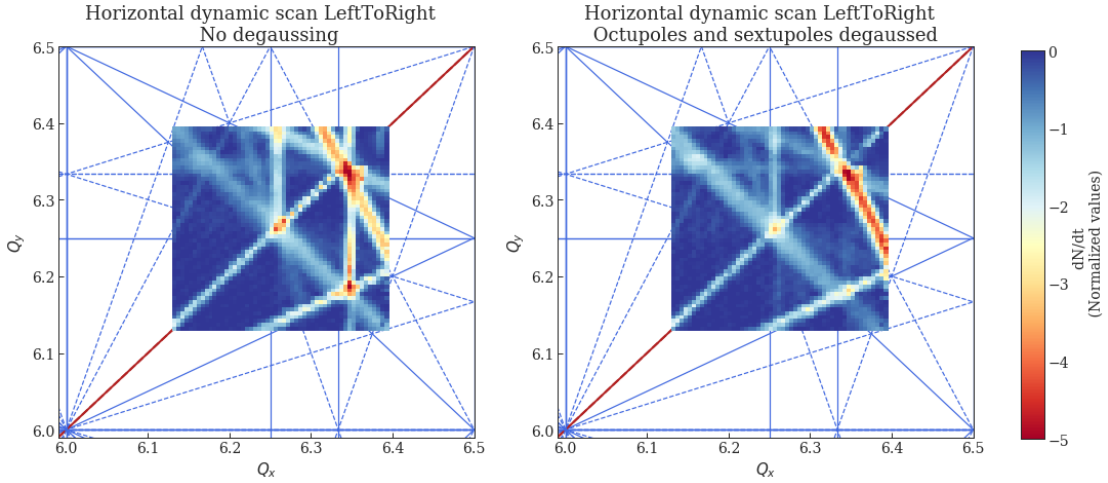

Figure 43: Left tune diagram illustrates a horizontal dynamic scan generated without degaussing any circuit, while the right one represents the case after the degaussing of octupoles and sectupoles.

A closer look at the data in Figure 44, proves what tune diagrams in Figure 43 yielded. The data yielded by these loss maps studies provide convincing evidence that the degaussing of the sextupoles and mainly of the octupoles had a significant impact on the elimination of 3rd and 4th order resonances. In Figure 44 we examine two resonances: the skew resonance $Q_x + 2Q_y = 1$ and the coupling $-Q_x + Q_y = 1$. Figure 44 compares the data on the intensities, amplitude and FWHM of the aforementioned resonances. In blue color it is described the non-degaussing configuration while in black the degaussing one. The diagrams demonstrating the amplitude the resonance, along the resonance itself, are composed of the results of both configurations, for smoothing the comparison procedure. Same principle follows the diagram concerning the FWHM.

The plot which concerns the amplitude of the skew resonance clearly evidences that its losses after the degaussing are eliminated. It is apparent, as the absolute value of losses before degaussing is greater. While at the same time, FWHM along the skew resonance seems not to be affected a lot. Only at the end of the resonance we see some discrepancies between the two configurations. It can be seen that FWHM of the resonance in the case before degaussing is greater at the last part of the resonance, which might me due to the appearance of more resonances in the vicinity of the skew one. This can be reasonably assumed, as by that point the degaussing did not occur so as to eliminate them, thus they contribute in the augmentation of the width the skew resonance.

Turning now to the coupling resonance, one could confirm by looking the plot of amplitude that there is a negligible influence of degaussing on losses. Apart from a specific part along the resonance, where losses after degaussing are greater. The unexpectedly observation could be justified if we have in mind that after the degaussing some resonances disappeared preserving in this way the intensity of the beam, until she encounters the coupling resonance. Hence, the observed increase could be attributed to the fact that more particles of the beam, will meet the coupling resonance thus more losses would occur. Unlike the amplitude of the coupling resonance, FWHM maintain more or less the same value before and after the degaussing.

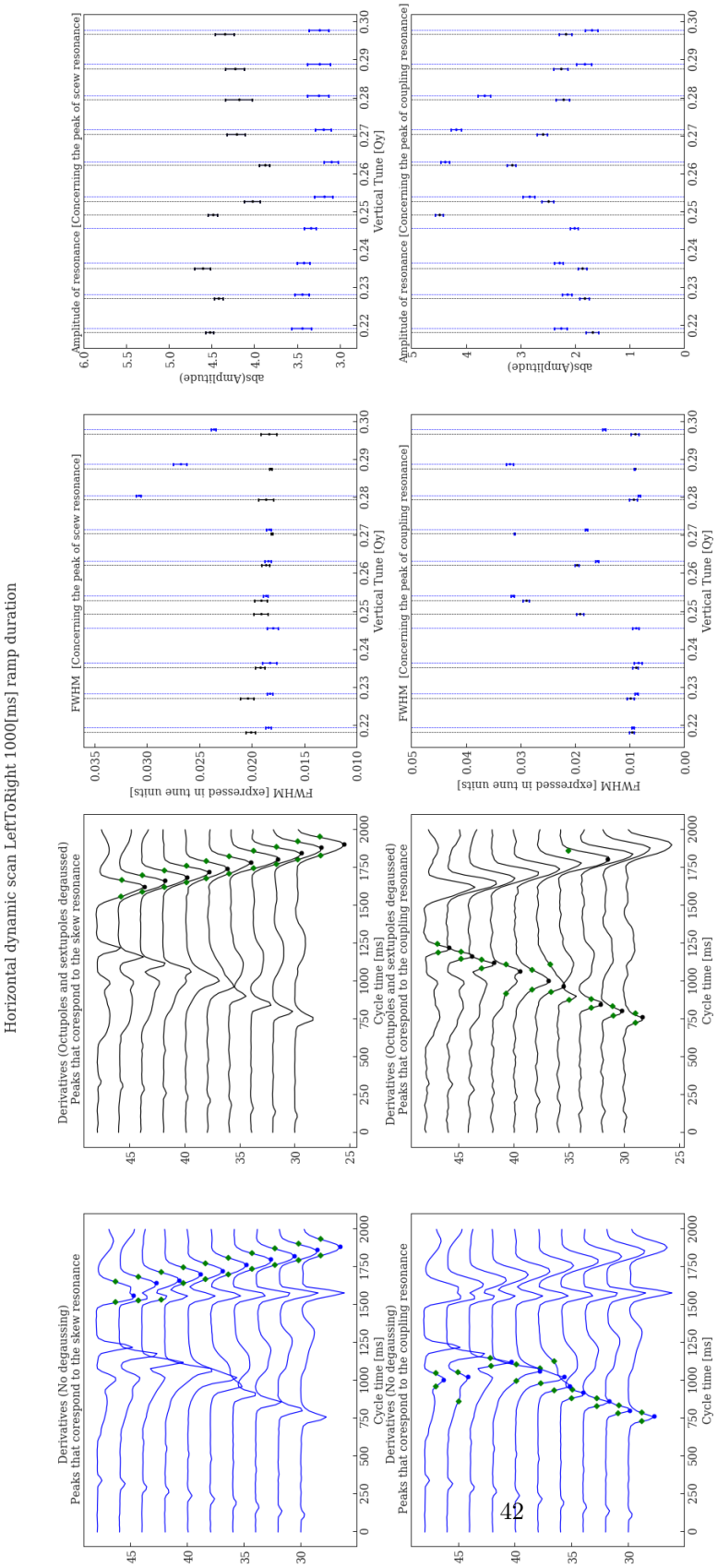

Figure 44: Horizontal dynamic scan. FWHM and amplitude of the skew resonance and the coupling one, before and after degaussing.

5.2 Degaussing of the main magnets

Coupling resonance was of a considerable importance thus it was intensively studied. In the following experiments we explore what is the main contributor of this resonance. Previous experiments showed that the coupling resonance could not be mitigated after the degaussing of octupoles and sextupoles. Further investigation followed in order to verify the circuit which generates it. In this experiment, due to the nature of this resonance much attention had given in the main magnets, which constitute a major part of PS, thus might be the reason of the beam losses which stem from the coupling resonance.

It is plausible that a number of limitations, concerning the currents applied on PFW, could not provide us a sufficient result.

Overall, the difference between the two cases is quite small given that PFW currents had an important current contribution in the main magnets. Loss maps obtained from scans in four different directions in Figure 45 while the values which are plotted in the diagrams constitute the average intensity.

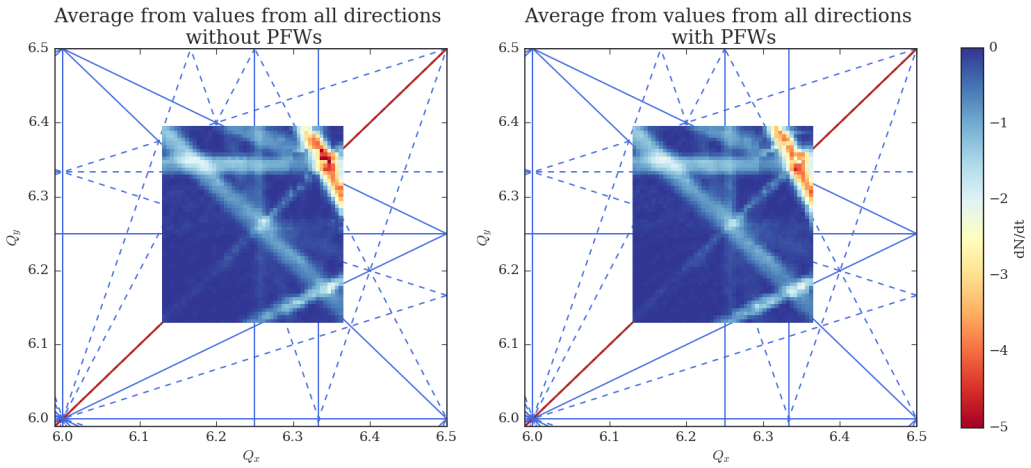

Figure 45: Left tune diagram is generated without degaussing any circuit, while its values are derieved from the mean values of dynamic scans in the four different directions, the right one represents the case after the degaussing of the main magnets using PFW.

Looking carefully the Figure 45, we evidently see now some differences between the two cases. The observations support the hypothesis stated at the outset that the degaussing of the PFW could have an impact in the main magnets. The BCT curves show the decreasing intensities, from which it is observed a small difference in the two curves. In the case of the degaussing it seems that the losses are less than the case which we did not degauss the PFW. Additionally, the derivative of the intensity curve (Figure 47) unveils different resonance reaction between the two cases. Accordingly, given the above we were forced to maximize the amplitude of the PFWs' currents.

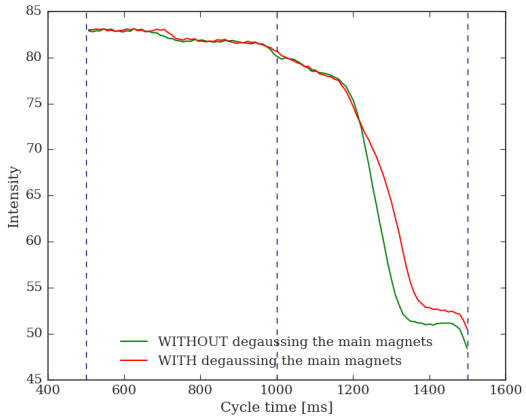

Figure 46: Intensity of the BCT signal for a fixed vertical tune of 6.18, at BCMS low-chromaticity configuration.

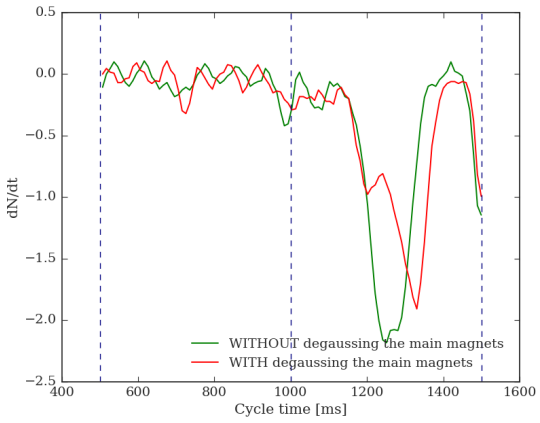

Figure 47: Derivative of the BCT signal for a fixed vertical tune of 6.18, at BCMS low-chromaticity configuration.

According to the previous experiemental set up, the impact of PFW to degauss the main magnets was negligible. Further research had been conducted to verify the previous results. At this point, the procedure would be done by choosing the maximum currents that PFW can accommodate.

Considerable attention must be paid, by the time this set up would be launched, as PFW consist a major part of PS thus a potential mismanagement of PFW currents could lead to problems in the operation of the machine. For this reason, the augmentation of the currents' amplitude had done gradually.

In the initial stage of the process, the degaussing cycles were programmed according to power converter limitations in terms of dI/dt. The performance was slightly unsatisfactory. This was probably as a result of the difficulties in repeating the degaussing many times due to restrictions come from the slope dI/dt. As anticipated, the rapidly way of amplitude decay explains why the final results was not as promising as we wanted to.

After the application of the new current scheme in the PFW, the experiment was relaunched.

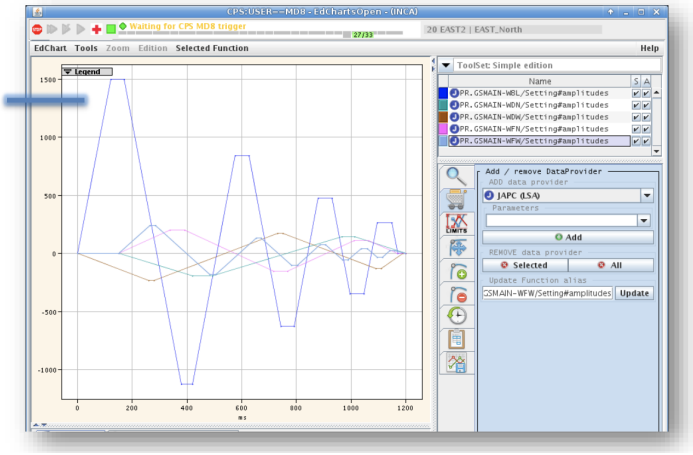

Figure 48: Functions of PFW maximum currents to degauss the main magnets.

Since we had adjusted the currents to their maximum values we expected a different resonance behaviour. The beam's loss maps presented in Figures 51,52, is the outcome of a meticulous processing which finally lead to interesting results. Tune diagrams represent the normalized values of loss rate. That means that each resonant line describes the losses which have corresponds each time to the residual intensity of the beam before meets the resonance. Despite the limitations of this method, and consequently the poor results in this configuration, our findings do nevertheless suggest that PFW are not so efficient in degaussing the main magnets. Especially, if we examine the skew resonance $Q_x + 2Q_y = 1$, we conclude to the fact that losses seem to be slightly reduced after the degaussing. More details could be observed if we evaluate each resonant excitation scheme sepeartely.

On the basis of the evidence that the resonant excitation is different in the case of the degaussing, it seems fair to suggest a detail research in the intensity and the derivative curves of losses separately. As it is presented in Figures 51,52 the analysis focuses on two resonaces the skew resonance $Q_x + 2Q_y = 1$ and the coupling $-Q_x + Q_y = 1$. In the present study, the issue under scrutiny is to which extend the underlined resonances are affected before and after degaussing. Figure 51,52 which correspond to a horizontal and a vertical scan respectively, corroborates the hypothesis by illustrating negligible discrepancies in the amplitude of resonance between two configurations. While the observed decrease in the FWHM in the case of degaussing the main magnets could be interpreted as being a result of the impact of the use of PFW.

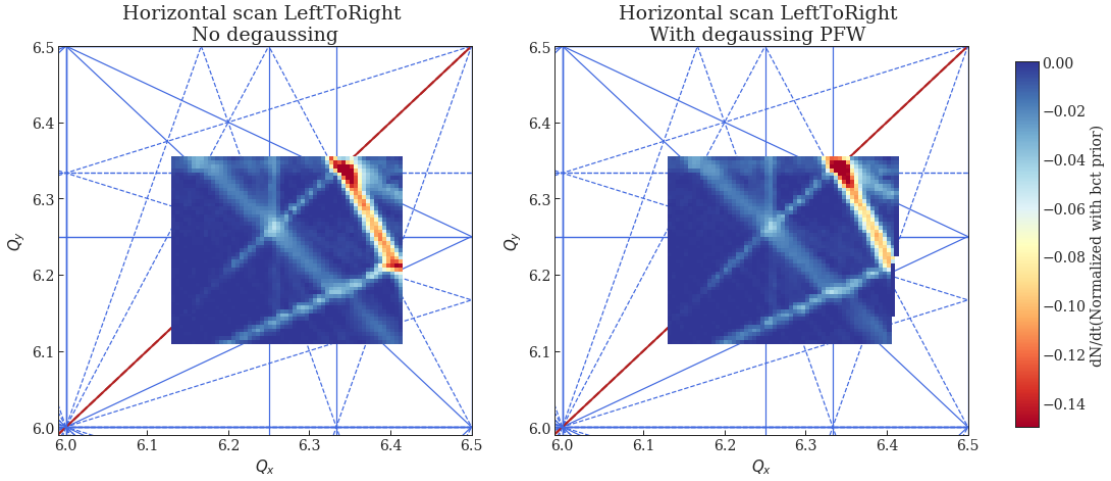

Figure 49: Left tune diagram illustrates a horizontal dynamic scan generated without degaussing any circuit, while the right one represents the case after the degaussing of the main magnets.

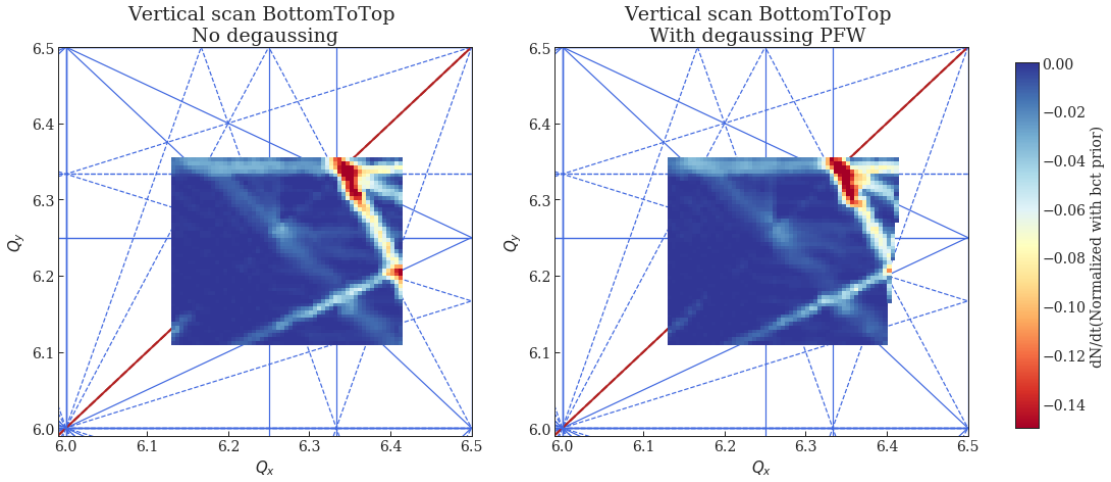

Figure 50: Left tune diagram illustrates a vertical dynamic scan generated without degaussing any circuit, while the right one represents the case after the degaussing of the main magnets.

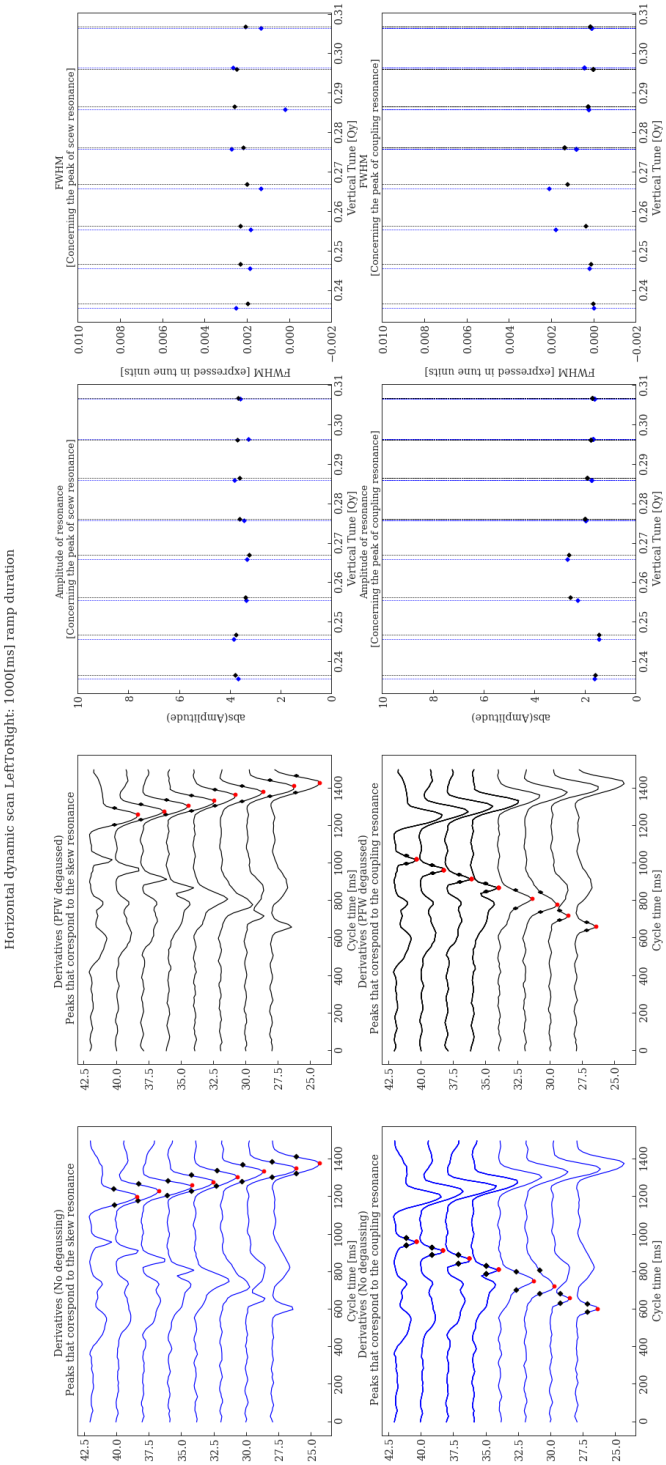

Figure 51: FWHM and amplitude of the skew resonance and the coupling one, before and after degaussing, concerning a horizontal scan.

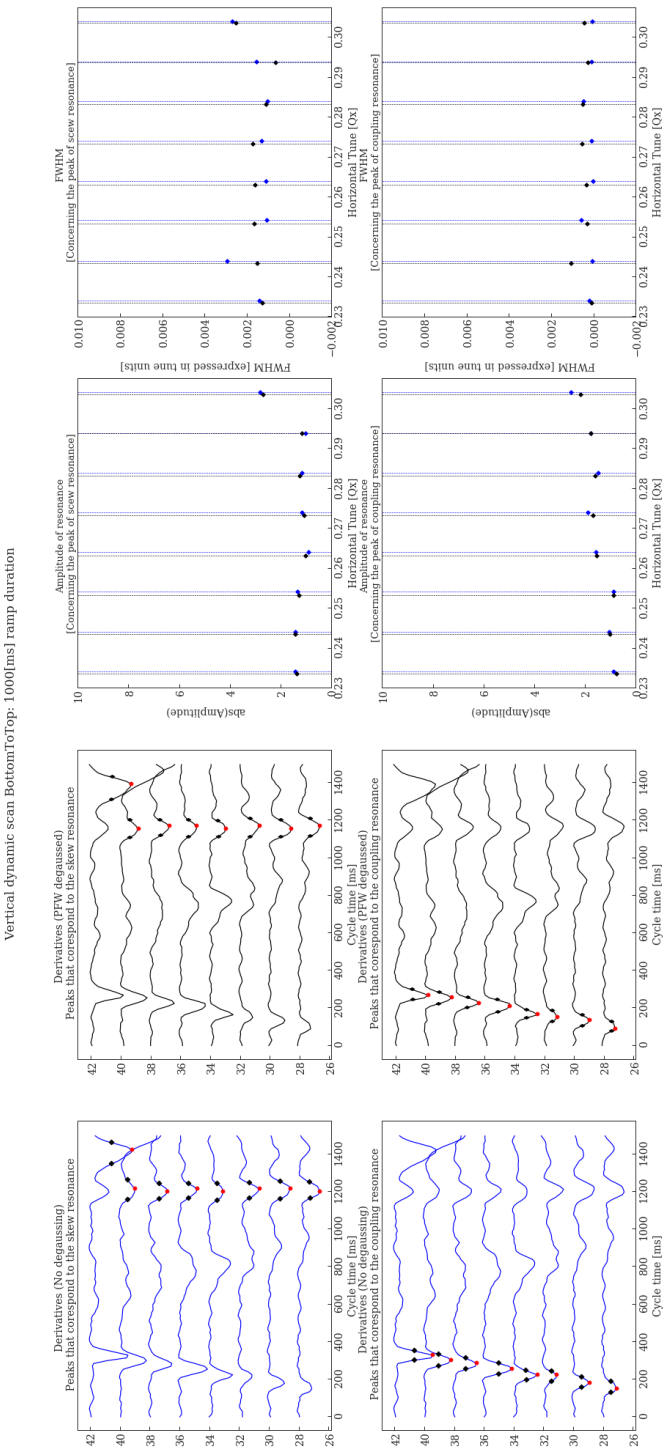

Figure 52: FWHM and amplitude of the skew resonance and the coupling one, before and after degaussing, concerning a vertical scan.

5.3 Conclusion

Remanence is the remaining magnetic field found in the material after the applied magnetic field is reduced to zero. Imperfections in the magnetic field in alliance with the remanence can inevitable lead to resonant conditions thus introduce emittance growth which may result to severe beam losses. Experiments on demagnetization of some dedicated multipoles were carried out, in 2018 in order to better investigate the tune diagram resonant lines. Especially, remnant fields in octupoles and sextupoles used for MTE appeared a good candidate to explain the additional horizontal resonances. In operation, in order to demagnetize the multipoles, the degaussing technique was implemented. Firstly, we have managed to degauss both octupoles and sextupoles, then octupoles alone. All in all, we indeed see a qualitative difference in the two cases, concluding that octupoles seem to be main contributors in the resonances, while less impact of sextupoles was observed.

Coupling resonance was of a considerable importance, as previous experiments showed that it could not be mitigated after the degaussing of octupoles and sextupoles. Consecutively, it was intensively studied, in order to verify the circuit which generates it. In this experiment, due to the nature of this resonance much attention had given in the main magnets, which constitute the major part of the PS. There had been an attempt to degauss the main magnets by using PFW, however results prove that the use of PFW to degauss the main magnets did not have much impact on the resonances. The upshot of this research, is that PFW are not so efficient to degauss the main magnets.

6 Impact of changing the resonance crossing speed

Tune scans clearly revealed a couple of resonances. In general tune scans performed using a large emittance beam, injected directly from PSB. Then either the horizontal or vertical tune varied in the PS dynamically having a constant slope, so the beam was circulating around PS for 1000[ms]. One could wonder what would be the aftermath of a change in the slope of the tune ramp. Especially, what would be the impact on resonances in we cross them faster or slower. To this end, dedicated tune scans were performed with the purpose of investigating the impact of resonance crossing speed on the resulting tune diagrams. Our experimental set up bears a close resemblance to the one it was previously referred.

6.1 Measurement principle

In order to compare resonances' behaviour, our steps proceed very much in the same way as previous tune scans had done before. In the initial stage of the process closed orbit was corrected, so as to accurately execute all the measurements that will be discussed. The experiment proceeds following the steps outlined below. We focus on three different configurations, in which the horizontal tune was varied dynamically for three different time durations respectively. Firstly, we injected a bunch with large transverse emittances from PSB, keeping it on a flat bottom (1.4 GeV) between (500-1000)[ms], then between (500-1500)[ms] and finally between (500-2000)[ms]. In the first step we did the standard dynamic scan which lasted for 1000[ms]. Then took place a dynamic scan which lasted for 500[ms], which means that the slope of the ramp is now larger and consecutively we scan more fast as we scan for a sorter time now (500[ms]). Last but not least we ramp the horizontal tune for 1500[ms], meaning that the slope is now smaller with respect to the standard configuration, as the time duration of the ramp is now longer, therefore the scan is conducted slower. With the completion of these steps and after setting the appropriate matlab file we observe the programmed measurements. After collection of the data, they transferred to a python file in which data analysis took place. Finally, loss maps obtained from the derivative values of intensity in correlation with the tunes, both horizontal and vertical.

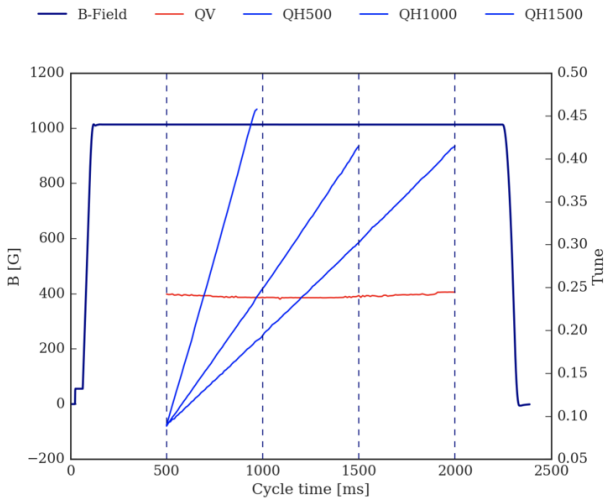

Figure 53: Measured magnetic field demonstrated in correlation with the three different configurations of horizontal tune scans (blue lines) against the cycle time[ms]. Vertical tune is kept constant in one plane while dynamically the horizontal tune is changed during the cycle.Then tune scans were performed aimed at the observation of the loss rate.

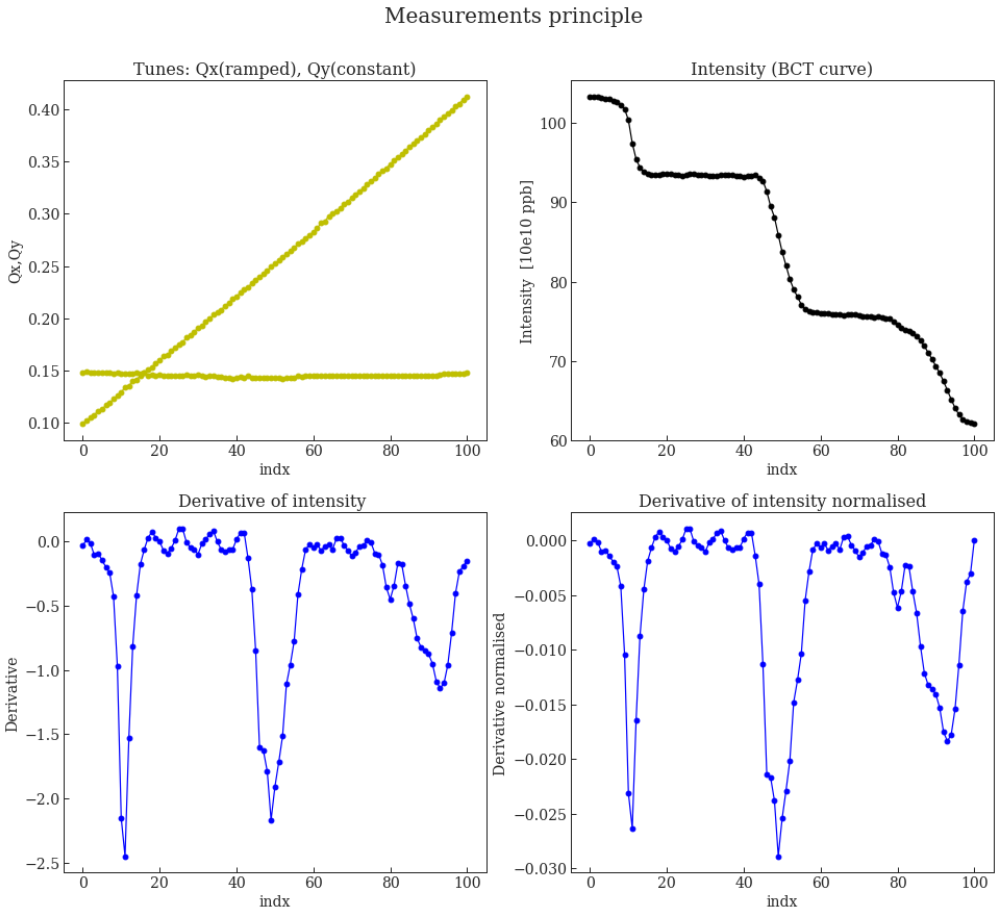

Figure 54: First plot (Up left), depicts an example of some measured tunes. Horizontal tune varied dynamically while the vertical one kept constant and increased with a specific step up to 0.4 each time it was supposed to be measured. Second plot (Up right) represents the BCT curve (Intensity [10e10 ppb]) along the cycle, from which we finally obtain the derivative curve which is depicted in the third plot (Down left). Last plot (Down right), concerns the normalized derivative values. Derivative values are normalized with the the intensity value with intensity value prior to each resonance crossing. Information about resonances derived from these derivative curves.

6.2 Investigating the origin of $3Q_x = 1$

According to results from the previous chapter, we were surprised to find that the degaussing of an octupolar circuit could extinguish resonances of 3rd order. So the conclusions of the review should be further interpreted with caution. The reason for this rather contradictory result is still can be attributed to a possible perturbation which occurs in the PS magnets the so called feed-down effect. In general, there are three main sources of perturbations in multipole fields which are the field error settings, energy errors of particles in the accelerator and feed-down errors. It is very likely that the field of strong super conducting magnets contains substantial multipole errors. Perturbations in magnets have different effects depending on what order the magnet has. But our interest concerns the feed-down errors. The feed-down effect occurs when a misaligned magnet of order N generates a magnetic field of order N-1. For example, a misaligned quadrupole gives a dipolar kick, or a misaligned sextupole gives a quadrupolar kick, etc. Accordingly, misalignement of a multipole could give additional field components to the multipole itself. The additional field components can generate extra focusing terms which create a major effect on the tune. Potential consequences of this include: resonances in particle motion from tune errors and beam size increase.

The effect of a misaligned multipole deflects the beam trajectory thus excites betatron oscillations. Therefore a study of the $3Q_x = 1$ resonance is very important to understand its source and possible mitigations in order to increase the machine's operational efficiency.

6.2.1 Correction of misalignement and closed orbit errors

As described in the previous section the effect of misaligned multipoles could lead to the feed-down effect thus to the appearance of additional order of resonances in each magnet. For this reason, orbit measurements are highly recommended. Good knowledge of the orbit is an essential precondition of the correction scheme. Correcting the beam's orbit could possible eliminate couple of existing resonances, as they might arise due to feed-down errors. Consequently, before the launch of loss-map measurements, orbit correction was necessary.

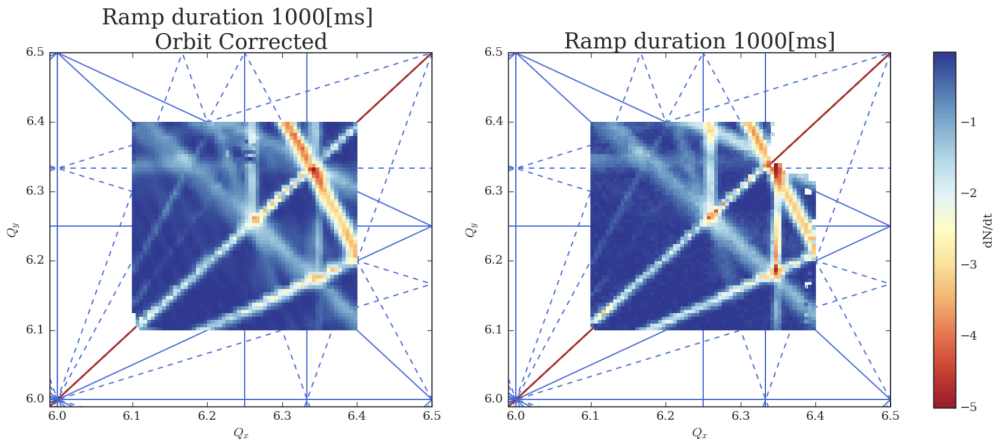

Figure 55: The effect of a misalignment of the magnet axis with the beam axis is clearly observed by looking the resonance discrepancies between the two tune diagrams.

It is interesting to notice that the $3Q_x = 1$ resonance was discovered to be excited as shown in Figure 55 (Right) , while it was not observed in the left tune diagram. This result has further strengthened our hypothesis that the $3Q_x = 1$ resonance appears to stem from ODN magnets due to feed down effects.

These results offer indisputable evidence for the reduction of the 3rd order resonance $3Q_x = 1$ after the orbit correction plus for the elimination of the strenght of the 4th order resonance $4Q_x = 1$.

6.3 Three different ramp durations

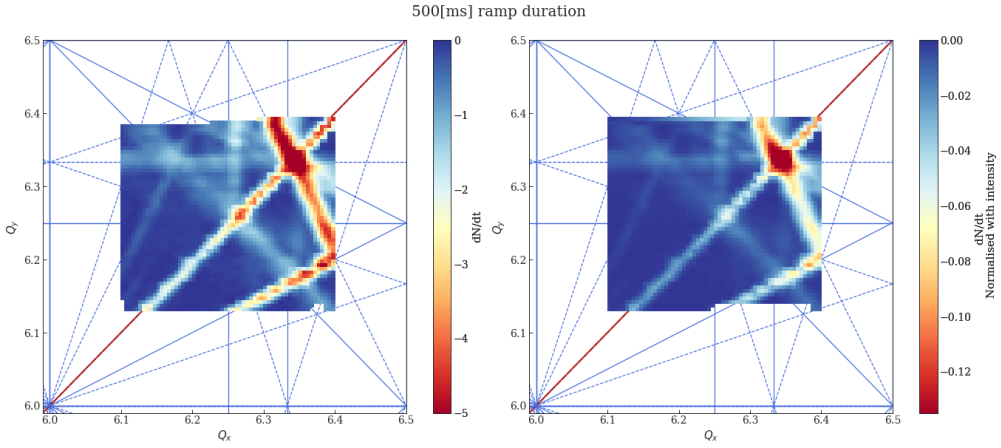

Figure 56: Left plot demonstrates a tune diagram generated from the derivative values of the intensity while the right one's generated from the normalized values of the intensity. Both plots represent measurements in which horizontal and vertical tune scans last for 500 [ms].

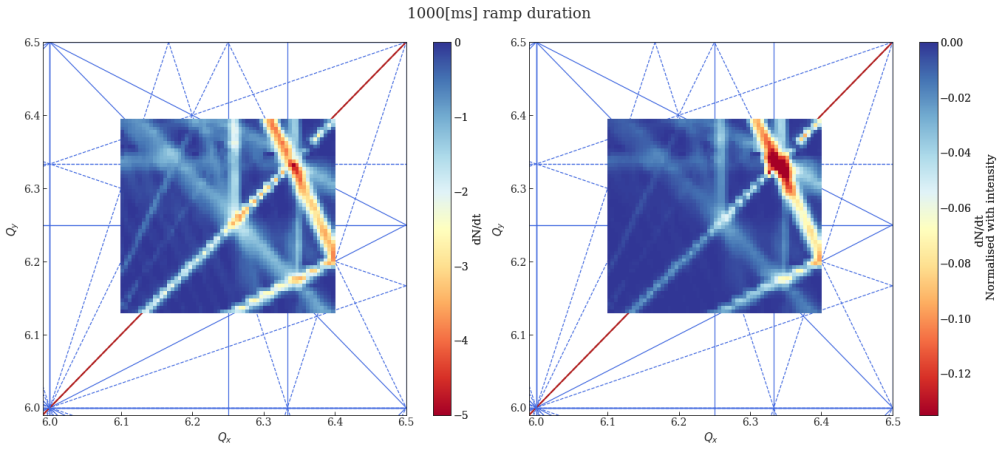

Figure 57: Again, left's tune diagram values derived from the derivative values of intensity while right's ones'from the normalized values. Here plots represent measurements in which horizontal and vertical tune scans last for 1000 [ms].

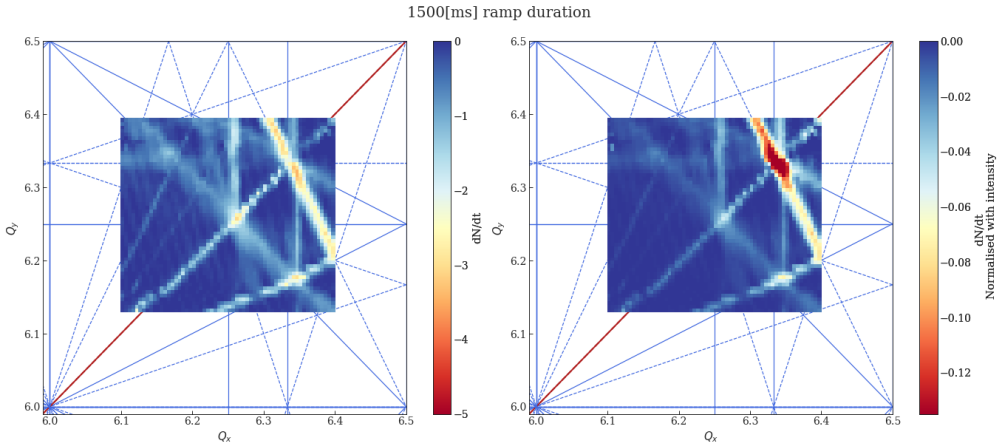

Figure 58: Here plots represent measurements in which horizontal and vertical tune scans last for 1500 [ms].

The previously demonstrated tune diagrams concern dedicated measurements which aimed to investigate the impact on resonances when changing the resonance crossing speed. Each pair of these loss maps corresponds to tune scans which have the same ramp duration. Left side plots generated from loss rate of the derivative of intensity while right side plots generated from loss rate of the normalised derivatives. We clearly observe that tune diagrams which are constructed out of the normalized derivatives represent more vicariously the strength of the resonance. In fact if we compare for each configuration the two cases of tune diagrams we clearly see the difference in the resonant intensity.

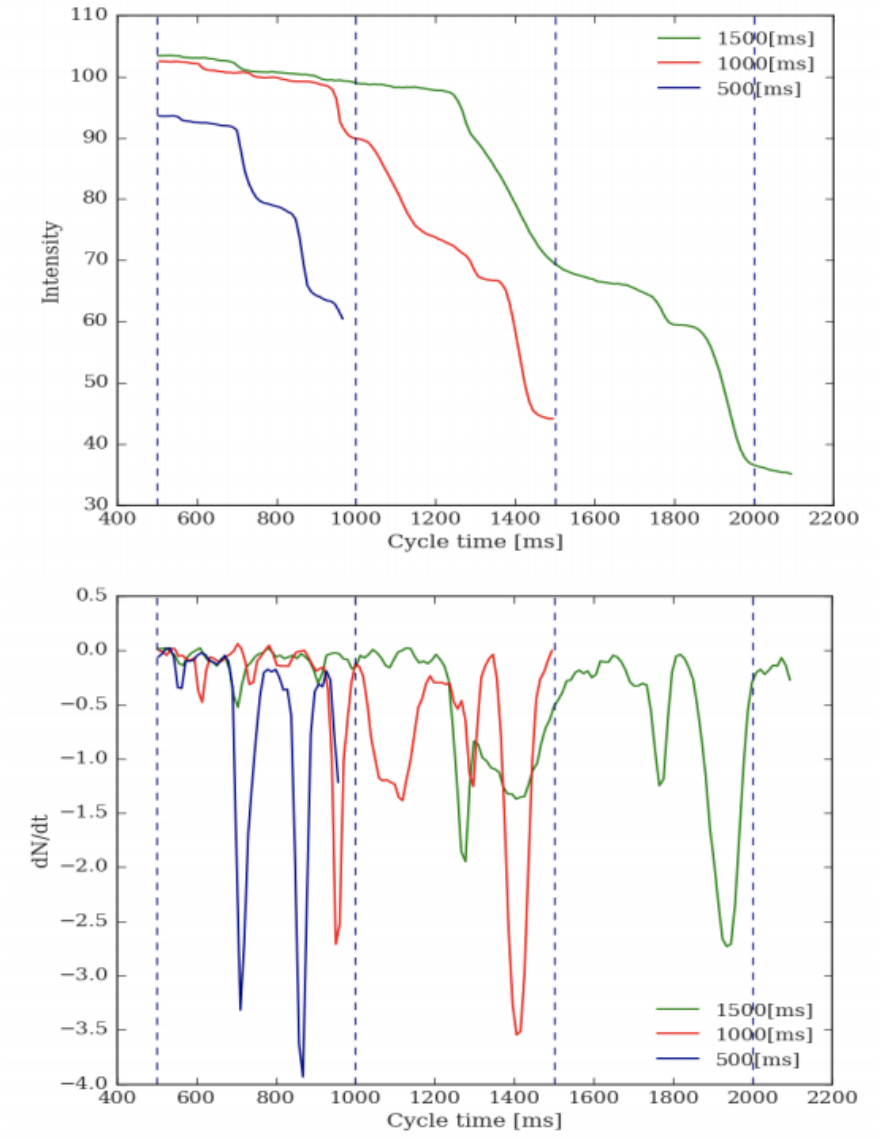

Figure 59: First plot (Up) illustrates the intensity diagrams around $Q_y = 6.30$ for the three different ramp durations, while the second plot (Down) shows the derivatives of the BCT signal for a fixed vertical tune of $Q_y = 6.30$.

From the graph which presents the derivatives we can note that more losses occur when resonant crossing speed is faster.

6.4 Summary of the three different configurations

As described in the previous section the effect of misaligned multipoles could lead to the feed-down effects thus to the appearance of additional order of resonances in each magnet. This effect occurs when a misaligned magnet of order N generates a magnetic field of order N-1.

According to results from the previous chapter, we were surprised to find out that the degaussing of an octupolar circuit could extinguish resonances of 3rd order like the $3Q_x = 1$ resonance. Apparently, further reasearch to clearly identify the origin of $3Q_x = 1$ resonance, needed to be done. A reasonable explanation for the origin of this resonace may be that it came from the feed down errors due to the misaligned multipoles. For the investigation of the previous mentioned resonane, orbit correction scheme was proposed. By the time closed orbit was corrected, we clearly observed the reduction in strength of the $3Q_x = 1$, $4Q_x = 1$ resonances. The results has further strengthened our hypothesis that the $3Q_x = 1$ resonance appears to stem from the misalinged octupolar magnets (ODN) which provoke feed-down errors.

Apparently, orbit correction took place, before the launch of the loss-map measurements in the three different ramp durations.

Tune diagram measurements revealed very different resonance excitation with respect to the resonance crossing speed. This work has revealed and concluded on the fact that resonances seem to be greater in strength when speed is fast. It can thus be suggested that strong coupling might be the main contributor for the significant resonances at 500[ms] duration.

7 Conclusions and outlook

This Master thesis work has been carried out at CERN in the framework of the LHC (Large Hadron Collider) Injector upgrade (LIU) program and also supported by National Technical University of Athens (NTUA).

The studies performed for this thesis led to design choices of the machine's shape, cell structure, transition energy, drift space allocations, the working point and to a thorough understanding of the factors relevant to the choices made.

Experiments were carried out in order to identify the existing betatronic resonances of Proton Synchrotron (PS) by applying a large emittance, not space-charge dominated beam on a magnetic flat bottom at constant energy, leading to the observation of the tune diagrams the so called loss maps. In other words this thesis focuses on studying loss maps in the PS and give an overview of the various resonant conditions.

As discussed in the introduction, studies have shown that an excited resonance can lead to emittance growth or beam loss due to the trapping mechanism. The trapping mechanism happens because particles cross the resonance as they follow the synchrotron motion, consequently the beam gets lost. Accordingly, the investigation of the existing resonances can draw important conclutions for the beams condintions when is launched in the machine at low energy.

It has been observed that different remnant magnetic fields which appear in some recently installed non-linear circuits, have a great impact on the resonances. It was therefore of a considerable interest to clarify possible changes in resonance strength overtime.

Another important factor to investigate the resonances in the PS, is the variety of applications making use of them. Paradoxically, some sets of multipole magnets are often required in a synchrotron to deliberately excite non-linear betatronic resonances. Dynamic scans had performed in this project in order to identify resonances and finally exploite them in a controlled way . For instance in order to extract the beam in a long slow spill CERN scientists use 3rd order resonances. Also, they use the 4th order resonances for the multi-turn extraction (MTE) scheme, which was invented to transfer the beam over 5 turns from the PS to the SPS at CERN with minimal losses.

Several types of tune scans were performed, because each direction reveals clearly different resonance excitation, for example a horizontal scan reveals in a very clear way vertical resonances.

This study has gone some way towards enhancing our understanding of resonance excitation, which seem to had been altered with respect to 2012 measurements. A potential explanation for this outcome could be the use of some new dedicated sextupoles for MTE instead of PFW, for chromaticity correction at low injection energy. From the research that has been carried out, it has been proved that remnant fields which could possibly stem from the use of specific non-linear magnetic fields (sextupoles, octupoles), could well be responsible for the new resonant conditions. Experimentally tested, that the chromaticity correction with dedicated sextupoles instead of PFW strongly excites additional resonances. Accordingly, these sextupoles cannot be used for operation as they excite too strong resonances.

Particular attention was paid to the remanence of the non-linear multipoles, which concerns the remaining magnetic field found in the material after the applied magnetic field is reduced to zero. PSs magnetic properties, introduce the hysteresis effects, indicating a major limitation on efficiency and operation of the beams. It is obtained that remanence, in alliance with the imperfections of the magnetic fields of PS, can inevitable lead to resonant conditions thus

introduce emittance growth which may result to severe beam losses. Experiments on demagnetization of some dedicated multipoles were carried out, in order to better investigate the tune diagram resonant lines. Especially, remnant magnetic fields in octupoles and sextupoles used for MTE appeared to be a good candidate to explain the additional horizontal resonances that were observed. To sum up, we could highlight the importance of the degaussing, as it reveals great impact on resonances.

Coupling resonance was of a considerable importance, as previous experiments showed that it could not be mitigated after the degaussing of octupoles and sextupoles. Consecutively, it was intensively studied, in order to verify the circuit which generates it. In this experiment, due to the nature of this resonance much attention had given in the main magnets, which constitute the major part of the PS. There had been an attempt to demagnitize the main magnets by using PFW, however results prove that the use of PFW to degauss the main magnets did not have much impact on the resonances. The upshot of this research, is that PFW are not so efficient in degaussing the main magnets.

Dedicated tune scans followed with the purpose of investigating the impact of resonance crossing speed on the resulting tune diagrams. But, before the launch of these measurements, there was a crucial need to correct the beams orbit, which was perturbating because of the misaligned multipoles. he effect of misaligned multipoles could lead to the feed-down effects thus to the appearance of additional order of resonances in each magnet. The main reason that induced us to re-fix the orbit was the first set of dynamic tune scans. That is because, results from these scans, revealed that resonances of 3rd order like the $3Q_x = 1$ resonance, could be strangely excited by an octupolar circuit. The outcome of the aforementioned measurements has further strengthened our hypothesis that the $3Q_x = 1$ resonance appears to stem from the misalinged octupolar magnets (ODN) which provoke feed-down errors.

By the time closed orbit was corrected, dynamic tune scans in three different time domains were launched. Tune diagram measurements of these scans revealed very different resonance excitation with respect to the resonance crossing speed. Summing up the results, it can be concluded that resonances seem to be greater in strength when speed is fast. It can thus be suggested that strong coupling might be the main contributor for the significant resonances at 500[ms] ramp duration.

Finally, our research could be a useful aid for LIU project whose target is to double the beam's brightness. According to the technical design report for LIU [3], the injection kinetic energy of the PS will be increased from 1.4 to 2 GeV to mitigate the large direct space charge tune spread of the increased brightness beams which can lead particles to cross many times betatronic resonances. Space charge effect constitutes a fundamental limitation for future research hence a close look at resonant lines of tune diagrams could possible be beneficial for LIU project.

References

[1] Alexander Huschauer. Working point and resonance studies at the CERN Proton Synchrotron, Sep 2012. Presented 10 Oct 2012.

[2] Francesco Velotti, Hannes Bartosik, Jeremie Bauche, Marco Buzio, Karel Cornelis, Matthew Fraser, and Verena Kain. Investigation of the Remanent Field of the SPS Main Dipoles and Possible Solutions for Machine Operation. (CERN-ACC-2017-180):THPAB146. 4 p, 2017.

[3] H Damerau, A Funken, R Garoby, S Gilardoni, B Goddard, K Hanke, A Lombardi, D Manglunki, M Meddahi, B Mikulec, G Rumolo, E Shaposhnikova, M Vretenar, and J Coupard. LHC Injectors Upgrade, Technical Design Report, Vol. I: Protons. Technical Report CERN-ACC-2014-0337, Dec 2014.

[4] Apollinari G., Béjar Alonso I., Brüning O., Fessia P., Lamont M., Rossi L., and Tavian L. *High-Luminosity Large Hadron Collider (HL-LHC): Technical Design Report V. 0.1.* CERN Yellow Reports: Monographs. CERN, Geneva, 2017.

[5] Jean-Paul Burnet, Christian Carli, Michel Chanel, Roland Garoby, Simone Gilardoni, Massimo Giovannozzi, Steven Hancock, Helmut Haseroth, Kurt Hübner, Detlef Küchler, Julian Lewis, Alessandra Lombardi, Django Manglunki, Michel Martini, Stephan Maury, Elias Métral, Dieter Möhl, Günther Plass, Louis Rinolfi, Richard Scrivens, Rende Steerenberg, Charles Steinbach, Maurizio Vretenar, and Thomas Zickler. *Fifty years of the CERN Proton Synchrotron: Volume 1.* CERN Yellow Reports: Monographs. CERN, Geneva, 2011.

[6] Raymond Wasef. 8th Order Super-Structure Resonance driven by Space Charge, Nov 2017. Presented 28 Jun 2018.

[7] Shriya Visavadia. Investigation into Possible Sources of Tune Jitter in the LHC, 2019. Presented 28 Jun 2019.

[8] Giulia Romagnoli, Jose Briz Monago, Mark Butcher, Marco Calviani, Denis Cotte, Yannick Coutron, Jaakko Esala, Edouard Grenier-Boley, Jan Hansen, Alexander Huschauer, Alessandro Masi, Francois-Xavier Nuiry, Didier Steyaert, Vasilis Vlachoudis, and S Gilardoni. Engineering Design and Prototyping of the New LIU PS Internal Beam Dumps. page WEPMG001. 4 p, 2018.

[9] A Huschauer, H Bartosik, S Hancock, and V Kain. Space charge and working point studies in the CERN Low Energy Ion Ring. pages 117–122. 6 p, 2017.

[10] A Huschauer, A Blas, J Borburgh, S Damjanovic, S Gilardoni, M Giovannozzi, M Hourican, K Kahle, G Le Godec, O Michels, G Sterbini, and C Hernalsteens. Transverse beam splitting made operational: Key features of the multiturn extraction at the CERN Proton Synchrotron. *Phys. Rev. Accel. Beams*, 20(6):061001. 15 p, 2017.

[11] Guido Sterbini, Jan Borburgh, Sanja Damjanovic, Simone Gilardoni, Massimo Giovannozzi, Cédric Hernalsteens, Michael Hourican, Alexander Huschauer, Karsten Kahle, Gilles Le Godec, and Olivier Michels. Performance of Transverse Beam Splitting and Extraction at the CERN Proton Synchrotron in the Framework of Multi-turn Extraction. (CERN-ACC-2016-174):THPMR043. 4 p, 2016.

[12] Alexander Huschauer, Jan Borburgh, Sanja Damjanovic, Simone Gilardoni, Massimo Giovannozzi, Michael Hourican, Karsten Kahle, Olivier Michels, Guido Sterbini, Cedric Hernalsteens, and Gilles Le Godec. Transverse beam splitting made operational: Recent progress of the multi-turn extraction at the CERN proton synchrotron. (CERN-ACC-2016-0100):MOPR009. 6 p, Jul 2016.

[13] Alexander Huschauer. Beam Dynamics Studies for High-Intensity Beams in the CERN Proton Synchrotron, May 2016. Presented 17 Jun 2016.

[14] Alexander Huschauer, Simone Gilardoni, and Raymond Wasef. Influence of the Alignment of the Main Magnets on Resonances in the CERN Proton Synchrotron. (CERN-ACC-2015-338):MOPJE046. 3 p, 2015.

[15] M Juchno. Magnetic Model of the CERN Proton Synchrotron Main Magnetic Unit. (CERN-ATS-2011-255):4 p, Dec 2011.

[16] D Tommasini. The PS Booster, PS and SPS Magnets for the next 25 years. This note provides information and analysis on the present status of the magnets installed in the CERN Proton Synchrotron Booster (PSB), the Proton Synchrotron (PS) and the Super Proton Synchrotron (SPS) in view of their possible operation for the next 25 years. Jan 2010.

[17] Django Manglunki and M Martini. Beam Optics Modeling at Cps Extraction Throughout A Nonlinear fringe field. *Part. Accel.*, 58(CERN-PS-97-015. CERN-PS-97-15. CERN-PS-97-015):209–219. 10 p, 1997.

[18] Matthew Fraser, Yann Dutheil, Vincenzo Forte, Ana Guerrero, Alexander Huschauer, Adrian Oeftiger, Salim Ogur, Federico Roncarolo, Eugenio Senes, and Frank Tecker. Matching studies between CERN PSB and PS through multi-turn beam profile acquisitions. page WEPMP025. 4 p, 2019.

[19] Alexandre Lasheen, Heiko Damerau, and Giorgia Favia. Uncontrolled Longitudinal Emittance Blow-Up during RF Manipulations in the CERN PS. *J. Phys.: Conf. Ser.*, 1067(CERN-ACC-2018-174. 6):THPAF041. 7 p, 2018.

[20] Vincenzo Forte, Simon Albright, Wolfgang Bartmann, Gian Piero Di Giovanni, Matthew Fraser, Christoph Heßler, Alexander Huschauer, and Adrian Oeftiger. Overview of the CERN PSB-to-PS Transfer Line Optics Matching Studies in View of the LHC Injectors Upgrade Project. page WEP2PO006. 6 p, 2018.

[21] Simone Gilardoni, Stephane Bart Pedersen, Caterina Bertone, Nicolo Biancacci, Alfred Blas, Dominique Bodart, Jan Borburgh, Paolo Chiggiato, Heiko Damerau, Sanja Damjanovic, James Devine, Tobias Dobers, Marine Gourber-Pace, Steven Hancock, Alexander Huschauer, Giovanni Iadarola, Luz Anastasia Lopez Hernandez, Alessandro Masi, Simon Mataguez, Elias Métral, Mauro Paoluzzi, Serena Persichelli, Serge Pittet, Stefan Roesler, Carlo Rossi, Giovanni Rumolo, Benoit Salvant, Rende Steerenberg, Guido Sterbini, Letizia Ventura, Joachim Vollaire, Raymond Wasef, Christina Yin Vallgren, and Mauro Migliorati. The PS Upgrade Programme: Recent Advances. page WEPEA042. 3 p, 2013.

[22] SS Gilardoni, S Bart Pedersen, C Bertone, N Biancacci, A Blas, S Damjanovic, D Bodart, J Borburgh, P Chiggiato, H Damerau, JD Devine, T Dobers, M Gourber-Pace, S Hancock, A Huschauer, G Iadarola, LA Lopez Hernandez, A Masi, S Mataguez, E Metral, M Paoluzzi, S Persichelli, S Pittet, C Rossi, S Roesler, G Rumolo, B Salvant, R Steerenberg, G Sterbini,

J Vollaire, R Wasef, L Ventura, C Yin Vallgren, and M Migliorati. The PS Upgrade Program: Recent Advances. (CERN-ACC-2013-0162):3 p, May 2013.

[23] G Rumolo, H Bartosik, V Kain, and M Meddahi. What to expect from the injectors during Run 3. Technical report, Geneva, Switzerland, 2019.

[24] Eugenio Senes, Jonathan Emery, Vincenzo Forte, Matthew Fraser, Ana Guerrero Ollacarizqueta, Alexander Huschauer, Federico Roncarolo, Jose Sirvent, Piotr Skowroński, and Frank Tecker. Transverse emittance measurement in the CERN Proton Synchrotron in view of beam production for the High-Luminosity LHC. (CERN-ACC-2019-093):MOPTS100. 4 p, 2019.